Title

Mutations in L-type amino acid transporter-2 support *SLC7A8* as a novel gene involved in Age-Related Hearing Loss.

Authors

Meritxell Espino Guarch[*,$,1,2,3], Mariona Font-Llitjós[$,2,4], Silvia Murillo-Cuesta[4,5,6], Ekaitz Errasti-Murugarren[3,4], Adelaida M. Celaya[4,5], Giorgia Girotto[7,8], Dragana Vuckovic[7,8], Massimo Mezzavilla[1], Clara Vilches[2], Susanna Bodoy[3,4], Ignasi Sahún[4,9], Laura González[2,4], Esther Prat[2,4,10], Antonio Zorzano[3,11,12], Mara Dierssen[4,9], Isabel Varela-Nieto[&,4,5,6], Paolo Gasparini[&,7,8], Manuel Palacín[*,&,3,4,11] and Virginia Nunes[*,&,2, 4,10].

[$] These authors contributed equally to this work

[&] These authors share leadership

* Corresponding authors

Affiliations

[1] Sidra Medical and Research Center, Experimental Genetics, Doha, Qatar.

[2] Molecular Genetics Laboratory- IDIBELL, Genes, Disease and Therapy Program. Barcelona, Spain.

[3] Institute for Research in Biomedicine (IRB Barcelona), The Barcelona Institute of Science and Technology, Barcelona, Spain.

[4] Biomedical Research Networking Centre on Rare Diseases (CIBERER), Institute of Health Carlos III, (U716, U730 and U731, Barcelona; U761, Madrid), Spain.

[5] Alberto Sols Biomedical Research Institute (CSIC/UAM), Madrid, Spain.

[6] Hospital La Paz Institute for Health Research (IdiPAZ), Madrid, Spain.

[7] University of Trieste, Department of Medicine, Surgery and Health Sciences, Trieste, Italy.

[8] Medical Genetics, Institute for Maternal and Child Health – IRCCS "Burlo Garofolo", Trieste, Italy.

[9] Center for Genomic Regulation (CRG), The Barcelona Institute of Science and Technology, Barcelona, Spain.

[10] Genetics Section, Physiological Sciences Department, Health Sciences and Medicine Faculty, University of Barcelona, Spain.

[11] Biochemistry and Molecular Biomedicine Department, Faculty of Biology, University of Barcelona, Spain.

[12] Biomedical Research Networking Centre on Diabetes and Associated Metabolic Diseases (CIBERDEM). Barcelona, (CB07/08/0017), Spain.

Abstract

Age related hearing loss (ARHL) is the most common sensory deficit in the elderly. The disease has a multifactorial etiology with both environmental and genetic factors involved being largely unknown. SLC7A8/SLC3A2 heterodimer is a neutral amino acid exchanger. Here, we demonstrated that SLC7A8 is expressed in the mouse inner ear and that its ablation resulted in ARHL, due to the damage of different cochlear structures. These findings make SLC7A8 transporter a strong candidate for ARHL in humans. Thus, a screening of a cohort of ARHL patients and controls was carried out revealing several variants in *SLC7A8*, whose role was further investigated by *in vitro* functional studies. Significant decreases in SLC7A8 transport activity was detected for patient's variants (p.Val302Ile, p.Arg418His, p.Thr402Met and p.Val460Glu) further supporting a causative role for SLC7A8 in ARHL. Moreover, our preliminary data suggest that a relevant proportion of ARHL cases could be explained by SLC7A8 mutations.

Keywords: *SLC7A8*, hearing loss, age-related hearing loss, knock-out mouse model, human mutations, auditory brainstem response, amino acid transporter.

Introduction

Age-related hearing loss (ARHL) or presbycusis is one of the most prevalent chronic medical conditions associated with aging. Indeed, more than thirty percent of people aged over 65 years suffer ARHL (1-3). Clinically, ARHL is defined as a progressive bilateral sensorineural impairment of hearing in high sound frequencies mainly caused by a mixture of 3 pathological changes: loss of the hair cells of the organ of Corti (sensory), atrophy of the stria vascularis (metabolic) and degeneration of spiral ganglion neurons (SGN), as well as the central auditory pathway (neural) (1, 4, 5). ARHL has a complex multifactorial etiology with both genetic and environmental factors contributing (6, 7). Although most people lose hearing acuity with age, it has been demonstrated that genetic heritability affects the susceptibility, onset and severity of ARHL (8-12). Unfortunately, the complexity of the pathology coupled with highly variable nature of the environmental factors, which cause cumulative effects, increases the difficulty in identifying the genetic contributors underlying ARHL. Most of the findings from genome-wide association studies (GWAS) performed into adult hearing function could neither be replicated between populations, nor the functional validation of those candidates be confirmed (13). Mouse models, including inbred strains, have been essential for the identification of several defined loci that contribute to ARHL (14).

SLC7A8/SLC3A2 is a Na^+-independent transporter of neutral amino acids that corresponds to system L also known as LAT2 (**L**-type **A**mino acid **T**ransporter-**2**) (15-17). SLC7A8 is the catalytic subunit of the heterodimer and mediates obligatory exchange with 1:1 stoichiometry of all neutral amino acids, including the small ones (e.g., alanine, glycine, cysteine and serine), which are poor substrates for SLC7A5 (18),

another exchanger with system L activity. Functional data indicate that the role of SLC7A8 is to equilibrate the relative concentrations of different amino acids across the plasma membrane instead of mediating their net uptake (15, 19, 20). The SLC7A8/SLC3A2 heterodimer is primarily expressed in renal proximal tubule, small intestine, blood-brain barrier and placenta, where it is thought to have a role in the flux of amino acids across cell barriers (16, 21-23). So far, SLC7A8 research has been focused mainly on amino acid renal reabsorption. However, *in vitro* studies demonstrated that SLC7A8 could have a role in cystine efflux in epithelial cells and the *in vivo* deletion of *Slc7a8* in a mouse model showed a moderate neutral aminoaciduria (24), suggesting compensation by other neutral amino acid transporters.

Therefore, in order to better understand the physiology of SLC7A8, we generated null *Slc7a8* knockout mice (*Slc7a8*$^{-/-}$) (25) and (Figure 1-figure supplement 1A). Here, we describe the detection of a hypoacusic phenotype in the *Slc7a8*$^{-/-}$ mouse model and demonstrate that novel loss-of-function SLC7A8 mutations constitute a primary cause in the development of ARHL in a cohort of elderly people from two isolated villages in Italy.

Results

Slc7a8 ablation causes ARHL

SLC7A8 is highly expressed in the kidney, intestine and brain, and neither full-length nor truncated SLC7A8 protein were detected in membrane samples of *Slc7a8*$^{-/-}$ mice (Figure 1A). The Allen Brain Atlas (26) localizes mouse brain SLC7A8 to the cortical subplate, cerebellum, thalamus and olfactory bulb. Our results showed that SLC7A8 protein was localized to the plasma membrane of neuronal axons in different brain regions such as, the choroid plexus, subfornical organ, cerebral cortex and hypothalamus by immunohistochemistry (Figure 1-figure supplement 2A). This specific localization in the brain pointed to the possibility that the absence of the transporter could potentially lead to neurological disorders. Behavioral screening showed that absence of SLC7A8 in mice does not affect either learning or memory (Figure 1-figure supplement 3). In contrast, a significant reduction in latency was observed in the rotarod acceleration test indicating impairment in motor coordination in *Slc7a8*$^{-/-}$ mice (Figure 1-figure supplement 3G). Reaffirming poorer motor coordination performance in the *Slc7a8*$^{-/-}$ mice, an increased exposure to shock on the treadmill was also observed (Figure 1-figure supplement 3B). Interestingly, a marked impairment was observed in the pre-pulse inhibition of acoustic startle response, which assesses the response to a high intensity acoustic stimulus (pulse) and its inhibition by a weaker pre-pulse. The response to a 120 dB single-pulse was significantly reduced in *Slc7a8*$^{-/-}$ mice (Figure 1B). The higher threshold required for responding to the acoustic stimulus in the PPI tests in *Slc7a8*$^{-/-}$ animals could potentially be indicative of a hearing impairment or to a defect in the stress response signalling.

Response to stress is modulated by the hypothalamic-pituitary-adrenal axis via the release of corticosterone from the adrenal cortex (27). As SLC7A8 is expressed in the murine pituitary gland (Figure 1-figure supplement 2A and S3H), plasma corticosterone levels under stressing conditions were analyzed. No differences were observed in corticosterone levels at either basal conditions, nor under restraint stress in the *Slc7a8*$^{-/-}$ group, indicating a normal stress response in the absence of SLC7A8 (Figure 1-figure supplement 3I). Thus, a hearing impairment in *Slc7a8*$^{-/-}$ animals was considered the most probable cause of the differences observed in the acoustic startle response test (Figure 1B). The impact of the ablation of SLC7A8 on the auditory system was tested initially on mice with a mixed C57BL6/J-129Sv genetic background.

Auditory brainstem response (ABR) recording, which evaluates the functional integrity of the auditory system, was performed in *Slc7a8*$^{-/-}$ mice. Reinforcing our hypothesis, adult 4 to 6 month-old *Slc7a8*$^{-/-}$ mice showed significantly higher ($p \leq 0.01$) ABR thresholds in response to click stimulus, compared with age matched *Slc7a8*$^{+/-}$ and wild type mice, which maintain normal hearing thresholds (Figure 1C-E). The hearing loss observed in *Slc7a8*$^{-/-}$ mice affected the highest frequencies tested (20, 28 and 40 kHz) (Figure 1F). The analysis of latencies and amplitudes of the ABR waves in response to click stimuli, showed increased latency and decreased amplitude of wave I, but similar II-IV interpeak latency, in the *Slc7a8*$^{-/-}$ mice when compared with the other genotypes, pointing to a hypoacusis of peripheral origin without affectation of the central auditory pathway (Figure 1-figure supplement 4A to D).

Mice were grouped according to genotype, age and ABR threshold level and descriptive statistics calculated, showing that the penetrance of the hearing phenotype in the

Slc7a8$^{-/-}$ mice is incomplete (Figure 1D and E). Therefore, mice were classified according to their hearing loss (HL) phenotype, defining normal hearing when ABR thresholds for all frequencies were <45 dB SPL, mild phenotype when at least two thresholds were between 45-60 dB SPL and severe hypoacusis when at least two thresholds were >60 dB SPL. At 4-6 months of age, *Slc7a8*$^{-/-}$ mice showed either severe (37.5%) or mild (25%) hearing loss, whilst mice from the other genotypic groups did not show hearing loss (Figure 1E). Next we studied 7-13 month-old mice, 50% of *Slc7a8*$^{-/-}$ mice presented severe hypoacusis and the hearing loss spread to lower frequencies with age. *Slc7a8*$^{-/-}$ mice with hearing loss showed statistically significant differences in ABR parameters when compared to the other genotypes (Figure 1F). Moreover, 43% of *Slc7a8*$^{+/-}$ mice developed mild hearing loss at 7 – 13 months, whereas the age-matched wild type mice maintained intact hearing indicating a predisposition towards hearing loss in aged *Slc7a8*$^{+/-}$ mice (Figure 1E).

The onset and severity of ARHL is attributed to both environmental and genetic factors (6). As the environmental factors were well controlled in all the experiments; thus the phenotypic variability could be attributed as the consequence of individual genetic differences. Indeed, it has been described that several strains of inbred mice present a predisposition to suffer ARHL dependent on multiple genetic factors (28, 29). Here, the hearing loss phenotype was confirmed in a second mouse strain, the inbread C57BL6/J genetic background (Figure 1-figure supplement 5). Additionally, longitudinal study of *Slc7a8*$^{-/-}$ mice into the inbred C57BL6/J genetic background showed higher penetrance than the mixed background throughout the ages studied (Figure 2-figure supplement 2).

Localization and quantification of SLC7A8 in the inner ear

The presence of SLC7A8 has previously been reported in the mouse cochlea (30-32), and specifically localized to the stria vascularis by liquid chromatography tandem mass spectrophotometry and by Western blotting (31). Here, SLC7A8 was detected in wild type mouse cochlea by immunofluorescence supporting its localization to the spiral ligament and spiral limbus from the basal to the apical regions of the cochlea (Figure 2A and B). SLC7A8 immunolabelling was not observed in the stria vascularis. We observed an intense expression of SLC7A8 in the spiral ligament surrounding the stria indicating that the SLC7A8 epitope (Figure 1-figure supplement 1B) is either hidden or absent in the stria vascularis. Quantification of SLC7A8 expression in the cochlea showed half a dose of the transporter in the *Slc7a8*$^{+/-}$ than in wild type mice, and its ablation in *Slc7a8*$^{-/-}$ mice (Figure 2C). A closer study of SLC7A8 immunofluorescence showed that the transporter is also expressed in the spiral ganglia neurons area (SGN) (Figure 1-figure supplement 2B).

The early HL onset and the progressive ARHL phenotype observed in *Slc7a8*$^{-/-}$ and *Slc7a8*$^{+/-}$ mice respectively, prompted us to compare the expression of SLC7A8 in wild type cochlea at different ages (Figure 1D). Immunofluorescence quantification of SLC7A8 intensity at 2- and 12-months of age showed expression in the young mice and increased presence of the transporter in the older mice (Figure 2D). In the same line, *Slc7a8* mRNA quantification from cochlea extracts showed a progressive increased expression throughout mouse life (Figure 2-figure supplement 1A).

Lack of *Slc7a8* induced damage in the organ of Corti, spiral ganglion and stria vascularis

The cytoarchitecture of the inner ear was studied by hematoxylin/eosin staining (Figure 3), immunofluorescence (Figure 4 and S8) and mRNA detection of several cochlear markers (Figures 3D and S7). Most of the structures of the cochlear duct, including spiral ligament, spiral limbus, tectorial and basilar membranes showed a normal gross cytoarchitecture in the *Slc7a8*$^{-/-}$ mice. In contrast, in the basal turns of the cochlea we observed that 3 out of 6 *Slc7a8*$^{-/-}$ mice evaluated showed complete loss of hair cells and flat epithelia, while only one *Slc7a8*$^{-/-}$ mouse showed intact epithelia in the organ of Corti (Figure 3A). Likewise, loss of cells in the spiral ganglia, especially in the basal regions of the cochlea, was observed (Figure 3A). *Slc7a8*$^{-/-}$ mice at 4 to 7 months of age presented ~50% of cell loss in the spiral ganglion compared with wild type mice (Figure 3B). Decreased number of cells in the ganglia significantly correlates with ABR threshold and HL phenotype (Figure 3-figure supplement 1 and B). Concomitantly with the loss of hair cells and spiral ganglion (SG) nuclei in *Slc7a8*$^{-/-}$ mice, the messenger levels of cell type specific biomarkers, such as the potassium voltage-gated channels *Kcnq2*, *Kcnq3* and *Kcnq5*, and the transporter *Slc26a5,* which are expressed in the organ of Corti and SG were down-regulated respectively (Figure 3D and S7B).

Less densely packed cells in the spiral ligament were observed in *Slc7a8*$^{-/-}$ than in wild type mice (Figure 3A). Reinforcing this observation, the expression of Kir4.1, a potassium channel highly expressed in stria vascularis cells (33), was also dramatically reduced by 50% in *Slc7a8*$^{-/-}$ (Figure 4B and Figure 4-figure supplement 1A). Likewise, decreased expression of Kir4.1 marker correlates with HL phenotype (Figure 3-figure

208 supplement 1C). Phalloidin labelling of actin fibers in the basal cells of the stria
209 vascularis was also decreased 50% in the base of the cochlea (Figure 4C and S8B).
210 SLC7A8 is abundantly expressed in fibrocytes of the spiral ligament and limbus (Figure
211 2), accordingly the number of fibrocytes in the spiral ligament decreased by 2/3 and 1/3
212 in the null and *Slc7a8*$^{+/-}$ mice, respectively (Figure 3C). Moreover, mice with severe HL
213 phenotype showed 30% less number of fibrocytes in the spiral ligament (Figure 3-figure
214 supplement 1D). The expression of the transcription factor *Tbx18,* essential for
215 fibrocytes development and differentiation, was 50% less in *Slc7a8*$^{-/-}$ than in wild type
216 mouse cochleae (Figure 3D). In contrast, the expression of s100, fibrocyte types I and II
217 marker, did not show significant differences (Figure 4D and Figure 4-figure supplement
218 1C).

219 **Mutations in *SLC7A8* are associated with ARHL**

220 Once we associated mouse SLC7A8 transporter with deafness and identified it as a
221 potential ARHL gene, screening for mutations in human populations was initiated.
222 Whole genome sequencing (WGS) and audiogram test data obtained from 147
223 individuals from isolated villages in Italy were included in the study. The inclusion
224 criteria were people 50-year old or older with an audiogram test done at high
225 frequencies (Pure-tone audiometric PTA-H, 4 and 8 kHz). Individuals with pure-tone
226 average for high frequencies (PTA-H) greater than or equal to 40 decibels hearing level
227 (dB HL) were considered ARHL cases, whilst people with PTA-H less than 25 dB were
228 considered as controls. A total of 66 cases suffering ARHL and 81 controls were
229 selected. The gene-targeted studies conducted in this isolated cohort succeeded in
230 detecting 7 heterozygous missense variants (Table 1). Four of the variants:

p.Val460Glu (V460E), p.Thr402Met (T402M), p.Val302Ile (V302I) and p.Arg418His (R418C) belong to ARHL cases (see Audiogram in Figure 5-figure supplement 1A) and other three: p.Arg8Pro (R8P), p.Ala94Thr (A94T) and p.Arg185Gln (R185L) to the control group (see Audiogram in Audiogram in Figure 5-figure supplement 1B).

All the mutations found in *SLC7A8* cases and controls from isolated villages of Friuli Venezia Giulia exhibited different frequencies in comparison to public data bases, such as ExAC among others (see Table 1). According to ExAC database's constrain metrics (34), the gene shows evidence of tolerance of both loss of function (pLi=0) and missense variation (missense Z score= -0.14).

Functional studies of *SLC7A8* mutations

A structural model of human SLC7A8 protein built using the homologous protein AdiC (35) in the outward-facing conformation (36) (Figure 5-figure supplement 1C and D) was used to localize all of the mutations identified here. Interestingly, 3 of the 4 mutations found in ARHL patients were located in very striking places: i) V302 is a conserved amino acid located in the extracellular loop 4 which corresponds to the external lid that closes the substrate binding site when the transporter is open to the cytosol, ii) T402 is located in transmembrane (TM) domain 10 facing to the substrate binding site, and iii) V460 is located at the very end of TM domain 12, with potential interaction with the plasma membrane. In contrast, R418 is in the intracellular loop 5, between TM domain 10 and TM domain 11 and with no functional role described in transporters with the LeuT-fold (37). Thus, 3 of these mutations were promising candidates to affect the transporter function due to their crucial location.

253 *In vitro* functional characterization of variants present in patients with ARHL and controls
254 was performed by measuring amino acid uptake in HeLa cells co-transfected with the
255 heavy subunit CD98hc and Strep tagged-SLC7A8 wild type and variants (Figure 5). Co-
256 expression of the light (SLC7A8) and the heavy (CD98hc) subunits in the same cell
257 increases the plasma membrane localization of the transporter (36). All tested variants
258 showed expression levels comparable to those of wild type, except for V460E that
259 showed only 20% expression of wild type protein (Figure 5-source data 1), being the
260 only variant that did not reach the plasma membrane as indicated by the lack of co-
261 localization with wheat germ agglutinin staining (Figure 5A). Amino acid transport
262 induced by SLC7A8 was analyzed for wild type and the identified variants (Figure 5B).
263 All variants present in controls (R8P, R186L and A94T) conserved more than 80% of
264 alanine transport compared with wild type protein. Three variants found in patients with
265 ARHL showed diminished alanine transport activity: T402M and V460E presented little
266 residual transport activity (14.6±2.6% and 3.6±0.3% of wild type activity respectively)
267 and R418C showed 50.7±5.4% of wild type alanine transport. Surprisingly, V302I
268 presented similar alanine transport levels to wild type SLC7A8. Location of residue
269 V302 within EL4 (within the external substrate lid (Figure 5-figure supplement 1D) led us
270 to additionally measure a larger size SLC7A8 substrate, whose transport could
271 potentially be more compromised than that of a small substrate (e.g., alanine).
272 Interestingly, V302I transport activity of tyrosine was found to be only 40.0±1.6% of wild
273 type SLC7A8. Because the V302I mutation showed a substrate-dependent impact,
274 tyrosine transport in the other variants was also tested (Figure 5B). Other SLC7A8
275 variants found in patients with ARHL and controls showed similar decreased transport

activity for alanine and tyrosine. Thus, the SLC7A8-induced tyrosine transport was clearly defective in the four variants found in patients with ARHL, whereas it was barely affected (>85% of wild type transport activity) in the variants found in controls.

Discussion

Here, we show that loss of function of the amino acid transporter SLC7A8 is associated with ARHL in both humans and mice. Full ablation of SLC7A8 transporter in mice produced a hearing loss defect with incomplete penetrance affecting mainly high frequency sounds, a characteristic of ARHL (Figure 1C-F, S5 and S6). Interestingly, hearing loss severity increases with age in *Slc7a8*$^{-/-}$ mice (Figure 1C-F and S6). Similarly, *Slc7a8* heterozygous mice showed increased hearing loss penetrance with age, as indicated by the late onset of the phenotype (starting from 7 months onwards) (Figure 1E, S5 and S6). In addition, SLC7A8 expression in wild type cochlea rises during ageing (Figure 2D and S7A). In patients with ARHL we identified four SLC7A8 variants that showed loss of function of transport of tyrosine (Figure 5B). Altogether, these results indicate that full SLC7A8 function is needed to keep an optimal hearing function throughout life, with half a dose of SLC7A8 being enough to accelerate ARHL phenotype in mice and humans.

The hearing loss (HL) phenotype in the *Slc7a8*$^{-/-}$ mice has been confirmed on two genetic backgrounds (mixed C57BL6/J-129Sv; Figure 1, and inbred C57BL6/J; Figure 1-figure supplement 5). Interestingly, onset and penetrance, but not severity, was increased in the hearing loss trait of *Slc7a8*$^{-/-}$ mice in the pure C57BL6/J background (Figure 1-figure supplement 5). It is well-known that the C57BL6/J background carry a mutation in the *Cdh23* gene causing early onset of ARHL (38, 39). It is also worthwhile

to mention that all the inbred C57BL6/J mice used to perform the experiments in this research were positive for the ARHL susceptibility allele A/A in *Cadh23* (data not shown). Genetic linkage between both genes could be disregarded because both are located in different chromosomes (*Slc7a8* in Chr:14 and *Cdh23* in Chr:8). Therefore, non-additive severity of the hearing loss phenotype of *Slc7a8* ablation and *Cdh23* susceptibility allele suggests that both genes may share similar mechanisms of pathogenicity.

In line with the results observed in the mouse model, the four human mutations found in heterozygosis in ARHL patients showed a reduced SLC7A8 transporter activity meanwhile the mutations found in control group did not affect the transporter activity (Figure 5B). The predisposition of *SLC7A8* to host deleterious variants, as shown by the *in silico*-patterns of missense and loss of function tolerance, could be explained because its aberration affects age-related hearing function, but its ablation is neither vital nor affects the reproduction of the mice (*Slc7a8*$^{-/-}$ showed same frequency of siblings as expected, data not shown). Furthermore, the presence of mutations in both ARHL cases and controls in our cohort with higher frequencies in respect to public databases could be explained as a result of isolation and inbreeding in our individuals; as isolation in a population could lead to an enrichment of deleterious variants due to relaxation of purifying selection (40). We also noted that in ExAC the mutations found in controls have a mean frequency that is 7 times higher than the ones found in our cases, and we speculate that this could be an indirect hint of the higher deleteriousness of the variations found in our cases in respect to the controls. Thus, the present work points to *SLC7A8* as a strong candidate gene involved in ARHL induction and the presented data

322 suggest that a significant proportion (~3%) of ARHL cases could be explained by
323 SLC7A8 mutations making it one of the major players so far described.

324 SLC7A8 was localized in key cochlear structures: the spiral ligament, spiral limbus and
325 spiral ganglion (Figure 2A and S2B) likewise the three main pathological changes
326 described in the ARHL were observed in the absence of SLC7A8: the hair cells of organ
327 of Corti (sensory), the spiral ganglia (neural), and the spiral ligament and the stria
328 vascularis (metabolic) (Figure 3).
329 The spiral ligament contributes to cochlear homeostasis and is crucial for normal
330 hearing. Degradation of the spiral ligament can result in either one form of hereditary
331 deafness through *POU3F4* mutations at locus DFN3 (41) or in the loss of endocochlear
332 potential (EP) in presbycusis mouse models (42). In the spiral ligament, SLC7A8
333 expression was detected in fibrocytes, mostly in type I, close to the stria vascularis
334 (Figure 2). In addition, a reduced number of total cells was observed in both *Slc7a8*$^{-/-}$
335 and *Slc7a8*$^{+/-}$ mice (Figure 3C). Type I fibrocytes are interconnected with the adjacent
336 types II and V cells forming a gap junction-dependent cell system with a relevant role in
337 ion homeostasis [for a review, see (43)]. Deafness due to fibrocyte alterations has been
338 described, which indicates the importance of their integrity for appropriate hearing (41,
339 44-47). Nonetheless, s100 expression (Figure 4C) appeared to be unaffected in the
340 absence of SLC7A8. Interestingly, mutations in genes expressed in spiral ligament
341 fibrocytes could affect stria vascularis function causing deafness, such as the ablation of
342 the fibrocyte transcription factor *POU3F4* that causes loss of fibrocytes IV and V in the
343 spiral ligament, decreased cellular density in the stria vascularis and decreased
344 expression of Kir4.1 (48). As the stria vascularis regulates nutrient transport and ion

345 fluxes is responsible for the maintenance of the EP (49), which is the driving force
346 required for neurotransmission after acoustic stimulus (50, 51). We observed alterations
347 in the stria vascularis, decreased expression of Kir4.1 and the basal cell marker
348 phalloidin all correlating with HL phenotype in *Slc7a8*$^{-/-}$, and similar traits in *Slc7a8*$^{+/-}$
349 mice (Figure 3A, 4B-C and S9). Moreover, is described that the ablation of the T-box
350 transcription factor gene *Tbx18*, expressed in the spiral ligament, compromises
351 fibrocytes differentiation (47) and concomitant disruption of the architecture of the stria
352 vascularis with almost complete absence of the basal cell layer, and down-regulation of
353 Kir4.1 (52). Likewise, deletion of Pendrin (*SLC26A4*, PDS) ($Cl^-/I^-/HCO3^-$ anion
354 exchanger expressed in mouse fibrocytes) showed pronounced signs of vestibular
355 disease attributed to an altered EP (53). Concomitant with reported data, transcript
356 levels of both *Tbx18* and *Slc26a4* are down-regulated in the *Slc7a8*$^{-/-}$ mouse (Figure
357 3D). Therefore, if we assume a defect in ion homeostasis in the absence of SLC7A8,
358 we could expect an EP impairment that should also trigger vestibular damage. In line
359 with this assumption, we observed impaired balance during gradual acceleration in
360 rotarod test performance of *Slc7a8*$^{-/-}$ mouse (Figure 1-figure supplement 3G).
361 Altogether, the data presented suggests that the absence of SLC7A8 in fibrocytes might
362 contribute a metabolic component to the progression of hearing loss.

363 The reduction in the number of cells of the spiral ganglia in *Slc7a8*$^{-/-}$ mice to half of
364 those in wild type (Figure 3A and B) and its correlation with ABR threshold at high
365 frequencies (Figure 3-figure supplement 1) could be considered causative of neuronal
366 hearing loss (54), and the lack of expression of SLC7A8 in SG might directly contributed
367 to this neurodegeneration (Figure 1-figure supplement 2B). SG axons are part of the

368 auditory nerve and transmit signals from the organ of Corti to the brain. In addition, it
369 has been described that SG degeneration may result in hair cells and sensory hearing
370 loss (55-57). SLC7A8 is expressed in the SG but not in the organ of Corti. However,
371 *Slc7a8*$^{-/-}$ mice also showed loss of hair cells (Figure 3A) suggesting a potential negative
372 feedback from the damaged SG similar to those described (55-57).

373 SLC7A8/SLC3A2 exchanges all neutral amino acids except for proline (15), and
374 therefore either SLC7A8 ablation in mice or *SLC7A8* loss-of-function mutations in
375 humans can alter availability or concentration of a specific set of neutral amino acids in
376 cells (especially fibrocytes and neurons) of the spiral ligament, spiral limbus and spiral
377 ganglion. Three of the four ARHL mutations (T402M, R418C and V460E) showed
378 similarly compromised transport of the amino acids tested (alanine and tyrosine),
379 whereas V302I selectively showed a defect for the large amino acid tyrosine (Figure
380 5B). Mutation V302I, located within the external lid in the extracellular loop 4, might
381 result in a steric hindrance with bulky substrates when closing the substrate cavity in the
382 inward-facing conformation of the transporter. SLC7A8 loss-of-function might render
383 alterations in the cell content of bulky neutral amino acids like branched chain amino
384 acids or glutamine, which affect proteostasis and renewal of cell structures causing cell
385 stress (58, 59). Caloric restriction, that involves both an increased branched amino
386 content and protein degradation, showed an effective delay of age-related cochlear
387 neuron degeneration (60, 61). In any case, *Slc7a8*$^{-/-}$ cochlea presents signs of
388 unresolved chronic inflammation with up-regulation of *Il1b* and *Il6* mRNA (Figure 2-
389 figure supplement 1C) and reduced activation of macrophages (down-regulation of Iba1
390 protein) (Suppl. Figure S8D). As SLC7A8 is also expressed in macrophages (62) the

role of the immune response in the hearing loss associated with *Slc7a8*$^{-/-}$ mice deserves further attention.

SLC7A8 also transports thyroid hormones (TH) (63, 64) as well as the dopamine precursor L-DOPA (65, 66). Even though hypothyroidism causes hearing loss characterized by alterations in cochlear development (67) and L-DOPA showed a protective role for cochlea during aging (29), *Slc7a8*$^{-/-}$ mice showed neither hypothyroidism (24) nor alterations in L-DOPA plasma levels (data not shown). The lack of SLC7A8 might be compensated by other transporters like the main TH transporter MCT8 (68). Moreover, we cannot disregard a local impact of a shortage of L-DOPA in the cochlea, which could influence its maintenance, altering the protective role of this metabolite. Therefore, in the absence of SLC7A8, three elements could play a role in the hearing loss phenotype: neutral amino acids, thyroid hormones and/or L-DOPA. Characterization of new SLC7A8 mutations with substrate-dependent transport activity will be necessary to draw a definitive conclusion as to the molecular mechanism of the SLC7A8 substrates involved in ARHL.

Conclusion

The present work provides evidence that the amino acid transporter SLC7A8/SLC3A2 has a direct role in age-related hearing-loss (ARHL). The ablation of SLC7A8 in a mouse model causes deafness with ARHL characteristics, defective audition at high-frequencies with early onset in homozygotes and progressive worsening in heterozygotes with age. Identification of rare variants in *SLC7A8* gene together with amino acid transport loss-of-function in ARHL patients supports the concept that this

gene has a role in the auditory system in association with other genetic and/or environmental factors.

This study highlights amino acid transporters as new targets to study in largely uncharacterized hearing disorders. The description of *SLC7A8* as a novel gene involved in a complex trait such as ARHL demonstrates the importance of amino acid homeostasis in preserving auditory function and suggests that genetic screening should be extended to consider other amino acid transporters as potential new genes involved in cochlear dysfunction. Our results may enable the identification of individuals susceptible to developing ARHL, allowing for early treatment or prevention of the disease.

Methods

All key research resources described in this section are summarized in Table 2.

Mouse Protocols

Animal experimentation complied with the ARRIVE guidelines and was conducted in accordance with Spanish (RD 53/2013) and European (Directive 2010/63/EU) legislations. All protocols used in this study were reviewed and approved by the Institutional Animal Care and Use Committee at IDIBELL in a facility accredited by the Association for the Assessment and Accreditation of Laboratory Animal Care International (AAELAC accredited facility, B900010). Mice procedures were done according with scientific, humane, and ethical principles. The studied mouse model did not show phenotype differences comparing male and female. Thus, to ensure that our research represents both genders, the studies describes in this work were performed using both sexes equitably. The number of biological and experimental replicates is detailed in the legend of each figure.

Mouse Model

Generation of the null *Slc7a8* (*Slc7a8*$^{-/-}$) was done by gene disruption. A coding region that includes exon 1 of the *Slc7a8* gene was replaced for a neomycin resistance cassette by homologous recombination using a pBlueScript vector with 2 homologous arms (right: 6.1kb and left: 2.3 kb) and two resistances (neomycin and thymidine kinase) in 5' region of the gene (Figure 1-figure supplement 1A). ES cells transfection and microinjection experiments were done by GenOway (Lyon-France). Chimera mouse was outcrossed with a wild-type C57BL6/J mouse to obtain first generation (F1) of *Slc7a8* heterozygous (*Slc7a8*$^{+/-}$) in a mixed C57BL6/J-129Sv background. Intercross of

448 F1 resulted in the analyzed F2 generation, which contemplates the 3 genotypes: wild
449 type, *Slc7a8*$^{+/-}$ and *Slc7a8*$^{-/-}$ knockout mice. The pure inbred genetic background was
450 generated backcrossing *Slc7a8*$^{-/-}$ F1 mice in the mixed C57BL6/J-129Sv strain for 10
451 generations with pure C57BL6/J wild type mice alternating male and females to avoid a
452 genetic drift in the X and Y chromosomes.

453 **Genotyping**

454 Mice genotype was confirmed by triplex-PCR using DNA from the tail. Primers used
455 were forward: 5'GGAGCGATCTGCGGAGTGA3'; reverse:
456 5'ACAGAGTGCGCTCCTACCCT3' and reverse KO-specific:
457 5'CGGTGGGCTCTATGGGTCTA3', and Standard DNA polymerase (*Biotools*
458 Ref:10.002). The PCR products are 458 bp (wild type allele) and 180 bp (*Slc7a8*$^{-/-}$
459 allele) fragment.

460 **Protein analysis**

461 Protein analysis was done by Western blotting using total membrane~~s~~ samples. Frozen
462 tissues (50-100 mg) were homogenized in 5 mL of membrane~~s~~ buffer (25 mM HEPES –
463 4 mM EDTA – 250 mM sucrose – and protease inhibitors) and centrifuged at 10,000
464 rpm for 10 min at 4°C. Supernatant was centrifuged at 200,000xg for 1 h at 4°C. The
465 pellet was resuspended in 150 µL of membrane buffer using a 25G syringe. Pierce BCA
466 Protein Assay Kit (Thermo Scientific Ref:23225) was used for protein quantification.
467 Polyclonal rabbit antibody against mouse SLC7A8 protein was generated using an
468 antigen against the C-terminal region (peptide sequence: PIFKPTPVKDPDSEEQP)
469 (Figure 1-figure supplement 1B). Serum extracts from inoculated rabbits were purified
470 with protein G and used as primary antibody. Detection was by chemiluminescent

reaction using ECL (GE Healthcare Ref:RPN2232) and autoradiography (Amersham Hyperfilm Ref:28906839). For specific SLC7A8 light subunit detection, samples were run in the presence of 100 mM of dithiothreitol (SigmaAldrich Ref:D9779).

Behavior tests

Rotarod (Panlab Ref:LE8500).The experimental design consisted of two training trials (TR) at the minimum speed (4 rpm) followed of two different tasks: (a) motor coordination and balance were assessed by measuring the latency to fall off the rod in consecutive trials with increasing fixed rotational speeds (FRS 4, 10, 14, 19, 24, and 34 rpm). The animals were allowed to stay on the rod for a maximum period of 1 min per trial and a resting period of 5 min was left between trials. (b) In the accelerating rod test, the rotation speed was increased from 4 to 40 rpm during two sessions of 1 min. For each trial, the elapsed time until the mouse fell off the rod was recorded. **Treadmill** (Panlab Ref:LE8710MTS): During 2 training trials (TR), the inclination of the treadmill was increased from 0° to 20° from the horizontal plane at different speeds (5, 10, 20, 30, 40 and 50 cm/sec). Whenever an animal fell off the belt, foot shocks were applied for a maximal duration of 1 sec. After the shock, mice were retrieved and placed back. **Morris water maze** (MWM): Mice were tested over 4 days (4 trials/session, 10 min inter-trial intervals). The Morris Water Maze test consists of a circular tank (150 cm diameter, 100 cm high) filled with opaque water (with non-toxic white paint) and maintained at 21 ± 2ºC. A removable circular platform (8 cm diameter) was located in a fixed position (NE quadrant) inside the pool. The pool was surrounded by white curtains, with cues affixed. The test was performed under low non-aversive lighting conditions (50 lux). An overhead camera connected to video-tracking software (SMART, Panlab

494 SL., Spain) will be used to monitor the animal's behavior. Latency to reach the platform,
495 total distance travelled, speed and time in zones will be recorded for posterior data
496 analysis. The maze was surrounded by white curtains with black patterns affixed, to
497 provide an arrangement of spatial cues. A pre-training session was performed in which
498 the platform was visible in the center (day 1), followed by five acquisition sessions
499 during which the platform was submerged 2 cm below the water (days 2-6). In each
500 trial, mice were introduced in the pool from one of the random starting locations. Mice
501 failing to find the platform within 60 sec. were placed on it for 10 sec. At the end of every
502 trial the mice were dried for 15 min in a heater. Escape latencies, length of the
503 swimming paths and swimming speed for each animal and trial were monitored and
504 computed by a tracking system connected to a video camera placed above the pool.
505 **Pre-pulse inhibition of acoustic startle response** (PPI) (Panlab Ref:LE116): Training
506 was 5 min of habituation time to the apparatus with a background noise level of 70dB
507 and then exposed to six blocks of 7 trial types in pseudo-random order with 15 sec.
508 inter-trial intervals. The trials: 1 sec of a 120 dB, 8000kHz sound preceded 100 msec.
509 by a 40 msec pre-pulse (PP) sound of 74, 78, 82, 86 or 90 dB. The startle response was
510 recorded for 65 msec, measuring every 1 msec. from the onset of the startle stimulus.
511 **Restrain stressor** (LabResearch Ref:G05): Mice were habituated for 3 days prior the
512 experiment collecting 10-15 μL of blood from tail. All sets were carried in the same room
513 at the same time to minimize environmental variations and corticosterone fluctuations
514 as a result of circadian rhythms. Mice were placed for 15 min in the conditioning unit
515 and 75μL of tail's blood was collected. For recovery mice were placed into a clean cage
516 for 90 min. Blood corticosterone were determined by Corticosterone EIA kit (Enzo

517 Ref:ADI900097).

518 **Auditory Brainstem Response test (ABR)**

519 Hearing was evaluated by recording the auditory brainstem responses (ABR) with a
520 System 3 TDT Evoked Potential Workstation (Tucker Davis Technologies TDT,
521 Alachua, FL, USA) as previously described (69, 70). Briefly, mice were anesthetized
522 with intraperitoneal injection of ketamine (100 mg/kg) and xylazine (10 mg/kg), and
523 placed inside a sound chamber. Broadband click (0.1 ms) and tone bursts (5 ms) at 8,
524 16, 20, 28 and 40 kHz were delivered with an open field speaker (MF1, TDT) at an
525 intensity range from 90 to 10 dB sound pressure level (SPL) in 5–10 dB SPL steps. The
526 electrical responses were amplified and averaged and the ANABR recordings analyzed
527 with BioSig® software (TDT) to determine hearing thresholds in response to each
528 stimulus, peak and interpeak latencies and peak amplitudes. Animals were kept
529 thermostatized and monitored during both anesthesia and the following recovery period.

530 **Histology and Immunohistochemistry**

531 Mice were perfused through vascular system with 4% PFA and inner ear and brain
532 samples were collected. The cochlea was dissected, post-fixed and decalcified in 0.3 M
533 EDTA pH 6.5 (Sigma-Aldrich Ref:E1644) for seven days. Decalcified cochleae were
534 embedded in OCT or paraffin as reported (71). Deparaffinized cochlear sections were
535 stained with hematoxylin and eosin for general cytoarchitecture evaluation.

536 **Immunohistochemistry**: Floating brain tissue sections were incubated with 3% H_2O_2 in
537 10% methanol in PBS for 10 min. Blocking buffer with: 0.2% gelatine, 0.2% Triton x-100
538 and 10% FBS for 30 minutes. Primary antibody: anti-SLC7A8 1/500 in blocking buffer
539 ON at 4 °C with agitation. Secondary antibody: 1/200 biotinylated anti rabbit in blocking

540 buffer for 1h at RT. Third antibody: 1/100 of A+B conjugate (Vectastain, Ref:ABC kit) in
541 blocking buffer for 1 h at RT. Develop staining: 0.03%DAB in PBS for 5min. Reaction:
542 incubate 0.03%DAB + 1/10.000 H_2O_2 for 2-7 min with agitation. Reaction was stopped
543 by rinsing with PBS. Sections were dried and dehydrated before mounting. Detection
544 was using a bright-light microscope. **Immunofluorescence:** OCT tissue sections were
545 permeabilized by incubating for 10 min with 0.1% Triton X-100 and incubated as
546 reported (72, 73) with the following primary antibodies: anti-SLC7A8 (1/200), -s100
547 (1/1000, Sigma-Aldrich Ref:S2532), -Kir4.1 (1/200, Merck Millipore Ref:AB5818), -IBA1
548 (1/100, Abcam Ref:ab5076), or with Phalloidin (1/100, Thermo Fisher Scientific
549 Ref:A22287), ON at 4°C. Sections were then incubated with secondary antibodies:
550 (1:300, Thermo Fisher Scientific Ref:A-11034 Goat anti-Rabbit Alexa Fluor 488, Ref:A-
551 11030 Goat anti-Mouse Alexa Fluor 546, Ref:A-21206 Donkey anti-Rabbit Alexa Fluor
552 488, Ref:A-11056 Donkey anti-Goat Alexa Fluor 546) for 2h at RT. Detection by
553 confocal microscopy (Leica, Ref:LSM 780 Zeiss).

554 **Fluorescence quantification**

555 4 sections of apex, middle and basal turns of the cochlea were quantified using the
556 same settings, including argon laser voltage, for the quantification. Using Fiji software,
557 the sum of the intensity of all stacks (2.6 μm in the z axis along the 10 μm section) from
558 the spiral ligaments + stria vascularis area was extracted. Data were analyzed with
559 Prism 7 statistic software package (Graph Pad Software, Inc.). Statistical significance
560 was determined by Student's t test for unpaired samples. The number of biological and
561 experimental replicates are detailed in the legend of each figure.

562 **Quantitative RT-PCR**

563 RNA was isolated using RNeasy (Qiagen) from 1–2 cochleae; its integrity and
564 concentration were assessed using an Agilent Bioanalyzer 2100 (Agilent Technologies).
565 At least, three mice per condition were used. cDNA was then generated by reverse
566 transcription (High Capacity cDNA Reverse Transcription Kit; Applied Biosystems) and
567 gene expression analyzed in triplicate by qPCR using TaqMan Gene Expression Assay
568 kits (Applied Biosystems). The following probes were used: potassium voltage-gated
569 channel subfamily Q member 2 (*Kcnq2*) Mm00440080_m1; potassium voltage-gated
570 channel subfamily Q member 3 (*Kcnq3*) Mm00548884_m1; potassium voltage-gated
571 channel subfamily Q member 5 (*Kcnq5*) Mm01226041_m1; prestin (*Slc26a5*)
572 Mm00446145_m1; T-box transcription factor TBX18 (*Tbx18*) Mm00470177_m1;
573 interleukin 1 beta (*Il1b)* Mm00434228m1; interleukin 6 (*Il6)* Mm00446190m1; solute
574 carrier family 7 (cationic amino acid transporter, y+ system), member 8 (*Slc7a8)*
575 Mm01318971m1. PCR was performed on an Applied Biosystems 7900HT Real-Time
576 PCR System using *Hprt1 or RPLP0* as the endogenous housekeeping gene. Relative
577 quantification values were calculated using the 2-ΔΔCt method. All procedures have
578 been already reported (52).

579 **ARHL cohort recruitment and clinical assessment**

580 A total of 147 Subjects were recruited in North-Eastern Italy isolated villages (FVG
581 Genetic Park) (74) and from one isolated village from Southern Italy (Carlantino).
582 Subjects underwent a clinical evaluation to exclude any syndromic form of hearing loss
583 or other systemic illnesses linked with sensorineural hearing loss. Audiometric tests
584 using standard audiometers were carried out for each subject. Measurements have
585 been obtained after any acoustically obstructing wax was removed. Thresholds for six

586 different frequencies (0.25, 0.5, 1, 2, 4, 8 kHz) were measured and then a pure-tone
587 average for high frequencies (P-TAH) was computed by taking the average of 4 and 8
588 kHz. To avoid non-genetic variations in the hearing phenotype (e.g. monolateral hearing
589 loss), the best hearing ear was considered for each individual. Cases were defined as
590 people older than 50 years old having PTAH≥40, while controls were subjects more
591 than 50 years old with PTAH≤25.
592 All studies were approved by the Institutional Review Board of IRCCS Burlo Garofolo,
593 Trieste, Italy and consent forms for clinical and genetic studies have been signed by
594 each participant. All research was conducted according to the ethical standards as
595 defined by the Helsinki Declaration.
596 **Whole genome sequencing and mutation screening**
597 Blood samples were collected and used to extract DNA using standard protocols. Low
598 coverage whole genome sequence was generated using Illumina technology (Genome
599 Analyzer and HiSeq 2000) at the Welcome Trust Sanger Institute and Beijing Genomics
600 Institute. Data coverage was ranging from 4 to 10X. A multi-sample genotype calling
601 was performed and standard quality filters were applied. The detailed pipeline has
602 already been described elsewhere (75). Variants belonging to *SLC7A8* gene were
603 extracted using bcftools [http://samtools.github.io/bcftools/] and annotated with
604 ANNOVAR (76). Only the exonic variants were further considered. Finally, variants of
605 interest were confirmed by direct Sanger sequencing on a 3500 Dx Genetic Analyzer
606 (Life Technologies, CA, USA), using ABI PRISM 3.1 Big Dye terminator chemistry (Life
607 Technologies, CA, USA) per manufacturer's instructions. Mutation frequencies were
608 compared with public databases such as Esp6500siv2 (NHLBI Exome Sequencing

609 Project), 1000g (1000 Genomes Project), Campion (The Allele Frequency Net
610 Database) and ExAC (The Exome Aggregation Consortium). For SLC7A8 we collected
611 several statistics including the probability of loss of function intolerance (pLI), where the
612 closer pLI value is to 1, the more LoF intolerant the gene could be considered. We also
613 collected the missense Z score, a positive score indicates intolerance to missense
614 variation whereas a negative Z score indicates that the gene had more missense
615 variants than expected.

616 **Site-Directed Mutagenesis**

617 The QuikChange site-directed mutagenesis kit (Stratagene) was used to introduce point
618 mutations in SLC7A8 sequence, according to the manufacturer's protocol. The
619 pcDNA3.1-StrepTag fused SLC7A8 construct was used as template (77). Amino acid
620 substitutions were introduced into SLC7A8 sequence using a compatible reverse primer
621 and forward primers (Figure 5-source data 1). All primers annealed to the coding
622 sequence, and the position of the mutated codon was underlined. All constructs were
623 verified by DNA sequencing and then used for transient transfection.

624 **Cell culture and transfection**

625 HeLa cells (Sigma Aldrich, Ref: 93021013) were maintained at 37 ℃/5% CO2 in
626 Dulbecco's modified Eagle's medium (Life Technologies) supplemented with 10% (v/v)
627 fetal bovine serum, 50 units/ml penicillin, 50 µg/ml streptomycin, and 2 mM l-glutamine.
628 HeLa cells were transiently transfected with plasmid constructions mentioned above
629 with the use of *Lipofectamine* 2000 (Invitrogen) following the manufacturer's protocol.
630 Amino acid transport and fluorescence microscopy analyses were carried out 48 h after
631 transfection.

632 **Visualization of Strep-tagged amino acid transporters by fluorescence**
633 **microscopy**
634 To analyze the effect of the mutations on SLC7A8 protein expression and plasma
635 membrane localization, fluorescence microscopy of Strep-tagged wild type and mutant
636 transporters was performed on a semiconfluent monolayer of transfected HeLa cells
637 cultured on glass coverslips. Glass coverslip-grown cells were incubated with 1mg/ml
638 wheat germ agglutinin (WGA) labeled with Texas-Red (Thermo Fisher Scientific) at 37
639 ºC for 10 minutes, rinsed three times with phosphate-buffered saline-Ca^{2+}-Mg^{2+} and
640 fixed for 15 min in 4% paraformaldehyde. Fixed cells were blocked in blocking buffer
641 (10% FBS and 0.1% saponin in PBS) for 1h and then incubated for 1h with primary
642 antibody (anti-Strep Tag GT517, 1/100; Abcam). Secondary goat-anti-mouse-FITC
643 antibody (Life Technologies) was incubated for 2h protected from light and rinsed three
644 times with phosphate-buffered saline. Nuclear staining was performed by incubating 1
645 µg/ml Hoechst (Thermo Fisher Scientific) for 10 min, rinsed three times with phosphate-
646 buffered saline and then mounted with aqua-poly/mount coverslipping medium
647 (Polysciences Inc.). Images were taken using a Nikon E1000 upright epifluorescence
648 microscope. All images were captured during 200 ms except for those corresponding to
649 V460E that were overexposed to 2 s to reveal the subcellular localization of this very
650 low expressing variant. To quantify SLC7A8 wild type and mutated transporters
651 expression levels in cells, a single in-focus plane was acquired. Using ImageJ (v1.48,
652 NIH), an outline was drawn around each cell and area and mean fluorescence
653 measured, along with several adjacent background readings. The total corrected

654 cellular fluorescence (TCCF) = integrated density – (area of selected cell × mean
655 fluorescence of background readings), was calculated.

656 **Amino acid transport assay**

657 Amino acid uptake was measured by exposing replicate cultures at room temperature to
658 L- [^{3}H]-labeled alanine or [^{3}H]-tyrosine (1 µCi/ml; Perkin Elmer) in sodium-free transport
659 buffer (137 mM choline chloride, 5 mM KCl, 2 mM $CaCl_2$, 1 mM $MgSO_4$, and 10 mM
660 HEPES, pH 7.4). Initial rates of transport were determined using an incubation period of
661 1 min and 50 µM of cold alanine or tyrosine. Assays were terminated by washing with
662 an excess volume of chilled transport buffer. Cells were lysed using 0.1% SDS and 100
663 mM NaOH and radioactivity measured in a scintillation counter. Uptake values were
664 corrected by their total corrected cellular fluorescence (TCCF) for all transporters except
665 for V460E mutant, which does not reach the plasmatic membrane.

666 **Statistical analysis**

667 Behavior and ABR experiments using mice were not performed blind to genotype and
668 treatment conditions, but as data acquisition was automated this will not affect data
669 processing and analysis. The sample size was chosen according to the standard
670 sample sizes used in the field and without applying any statistical method. The general
671 criteria of exclusion were pre-established: 1) samples with a value that differed by
672 more/less than two standard deviations from the mean value were excluded from the
673 study. The statistical tests used in each experiment were appropriate to the type of
674 groups, data and samples. Unpaired Student t-test was used for experiments with only
675 two independent groups. Repeated measures 2-way ANOVA was applied when we had

to compare 2 independent groups (genotype as the between subjects factor) where repeated measurements of the dependent variable were obtained (Rotarod and PPI). Data were analyzed with IBM SPSS 23.0 statistic software package (Chicago, IL, USA). Statistical significance was determined by one-way analysis of variance (ANOVA) and Levene's F test to assess the equality of variances. When significant differences were obtained, post hoc comparisons were performed using Bonferroni or Tamhane tests to compare the three genotypes. Normal distribution of data and homogeneity of variances was assessed using Shapiro-Wilk and Levene tests, respectively. In most of the datasets these two assumptions were achieved. However, when not achieved and because we use comparable sample sizes and ANOVA is robust to normality violations, our results are still valid. Sphericity assumption was assessed using Mauchly's test and when not achieved Greenhouse correction was taken. Posthoc tests were performed using Bonferroni correction for individual comparisons. Bonferroni $P < 0.05$ was assumed as critical value for significance throughout the study. Statistical analyses were performed using SPSS package.

Acknowledgements

We thank to all volunteers that participate in this study, Professor Fernando Aguado for technical assistance in brain IHC, Professor Josep Chillarón for SLC7A8 antibody design, Dr. Miguel López de Heredia for critical reading of the manuscript, Saif Ahmed for the code to extract the images' analysis data, the core-facilities: IRB Advanced Digital Microscopy Facility (Anna Lladó and Julien Colombelli), the Genomics facility at the IIBm (CSIC-UAM), Units F1, F3 and F6-SEFALer (CIBERER) for their technical support and GenOway for the help in the homologous recombination and transfection of the construct into ES cells to generate the *Slc7a8*$^{-/-}$ mice. IRB Barcelona is the recipient of a Severo Ochoa Award of Excellence from MINECO (Government of Spain). M.D. acknowledges support of the Spanish Ministry of Economy and Competitiveness, 'Centro de Excelencia Severo Ochoa 2013-2017; M.D: and V. N. acknowledge the support of the CERCA Programme / Generalitat de Catalunya."

Bibliography

1. Gates GA, Mills JH. Presbycusis. Lancet. 2005;366(9491):1111-20.
2. Huang Q, Tang J. Age-related hearing loss or presbycusis. Eur Arch Otorhinolaryngol. 2010;267(8):1179-91.
3. Van Eyken E, Van Camp G, Van Laer L. The complexity of age-related hearing impairment: contributing environmental and genetic factors. Audiol Neurootol. 2007;12(6):345-58.
4. Schuknecht HF. Presbycusis. Trans Am Laryngol Rhinol Otol Soc. 1955(59th Meeting):401-18; discussion, 19-20.
5. Yamasoba T, Lin FR, Someya S, Kashio A, Sakamoto T, Kondo K. Current concepts in age-related hearing loss: epidemiology and mechanistic pathways. Hear Res. 2013;303:30-8.
6. Cruickshanks KJ, Nondahl DM, Tweed TS, Wiley TL, Klein BE, Klein R, et al. Education, occupation, noise exposure history and the 10-yr cumulative incidence of hearing impairment in older adults. Hear Res. 2010;264(1-2):3-9.
7. Christensen K, Frederiksen H, Hoffman HJ. Genetic and environmental influences on self-reported reduced hearing in the old and oldest old. J Am Geriatr Soc. 2001;49(11):1512-7.
8. Wingfield A, Panizzon M, Grant MD, Toomey R, Kremen WS, Franz CE, et al. A twin-study of genetic contributions to hearing acuity in late middle age. J Gerontol A Biol Sci Med Sci. 2007;62(11):1294-9.

9. Cruickshanks KJ, Klein R, Klein BE, Nondahl DM. Sunlight and the 5-year incidence of early age-related maculopathy: the beaver dam eye study. Arch Ophthalmol. 2001;119(2):246-50.

10. Gates GA, Couropmitree NN, Myers RH. Genetic associations in age-related hearing thresholds. Arch Otolaryngol Head Neck Surg. 1999;125(6):654-9.

11. Karlsson KK, Harris JR, Svartengren M. Description and primary results from an audiometric study of male twins. Ear Hear. 1997;18(2):114-20.

12. Cruickshanks KJ, Wiley TL, Tweed TS, Klein BE, Klein R, Mares-Perlman JA, et al. Prevalence of hearing loss in older adults in Beaver Dam, Wisconsin. The Epidemiology of Hearing Loss Study. Am J Epidemiol. 1998;148(9):879-86.

13. Payton PDaA. Genetics of Age-Related Hearing Loss. Genetics of Deafness. 2016;20(Basel, Karger):84–96.

14. Bowl MR, Dawson SJ. The mouse as a model for age-related hearing loss - a mini-review. Gerontology. 2015;61(2):149-57.

15. Pineda M, Fernandez E, Torrents D, Estevez R, Lopez C, Camps M, et al. Identification of a membrane protein, LAT-2, that Co-expresses with 4F2 heavy chain, an L-type amino acid transport activity with broad specificity for small and large zwitterionic amino acids. J Biol Chem. 1999;274(28):19738-44.

16. Rossier G, Meier C, Bauch C, Summa V, Sordat B, Verrey F, et al. LAT2, a new basolateral 4F2hc/CD98-associated amino acid transporter of kidney and intestine. J Biol Chem. 1999;274(49):34948-54.

17. Oxender DL, Christensen HN. Distinct Mediating Systems for the Transport of Neutral Amino Acids by the Ehrlich Cell. J Biol Chem. 1963;238:3686-99.

18. Mastroberardino L, Spindler B, Pfeiffer R, Skelly PJ, Loffing J, Shoemaker CB, et al. Amino-acid transport by heterodimers of 4F2hc/CD98 and members of a permease family. Nature. 1998;395(6699):288-91.

19. Meier C, Ristic Z, Klauser S, Verrey F. Activation of system L heterodimeric amino acid exchangers by intracellular substrates. EMBO J. 2002;21(4):580-9.

20. Verrey F. System L: heteromeric exchangers of large, neutral amino acids involved in directional transport. Pflugers Arch. 2003;445(5):529-33.

21. Bauch C, Forster N, Loffing-Cueni D, Summa V, Verrey F. Functional cooperation of epithelial heteromeric amino acid transporters expressed in madin-darby canine kidney cells. J Biol Chem. 2003;278(2):1316-22.

22. Kanai Y, Endou H. Heterodimeric amino acid transporters: molecular biology and pathological and pharmacological relevance. Curr Drug Metab. 2001;2(4):339-54.

23. del Amo EM, Urtti A, Yliperttula M. Pharmacokinetic role of L-type amino acid transporters LAT1 and LAT2. Eur J Pharm Sci. 2008;35(3):161-74.

24. Braun D, Wirth EK, Wohlgemuth F, Reix N, Klein MO, Gruters A, et al. Aminoaciduria, but normal thyroid hormone levels and signalling, in mice lacking the amino acid and thyroid hormone transporter Slc7a8. Biochem J. 2011;439(2):249-55.

25. Font-LLitjós M. Reabsorció renal d'aminoàcids: anàlisi de mutacions de SLC7A9, el gen de cistinúria de tipus B, i generació d'un model murí knockout de Slc7a8. Barcelona: Barcelona University (UB); 2009.

26. Science AIfB. Allen Mouse Brain Atlas San Diego, USA2004 [Available from: http://www.brain-map.org/.

772 27. Smith SM, Vale WW. The role of the hypothalamic-pituitary-adrenal axis in
773 neuroendocrine responses to stress. Dialogues Clin Neurosci. 2006;8(4):383-95.
774 28. Kane KL, Longo-Guess CM, Gagnon LH, Ding D, Salvi RJ, Johnson KR. Genetic
775 background effects on age-related hearing loss associated with Cdh23 variants in mice.
776 Hear Res. 2012;283(1-2):80-8.
777 29. Murillo-Cuesta S, Contreras J, Zurita E, Cediel R, Cantero M, Varela-Nieto I, et
778 al. Melanin precursors prevent premature age-related and noise-induced hearing loss in
779 albino mice. Pigment Cell Melanoma Res. 2010;23(1):72-83.
780 30. Yang Y, Dai M, Wilson TM, Omelchenko I, Klimek JE, Wilmarth PA, et al.
781 Na+/K+-ATPase alpha1 identified as an abundant protein in the blood-labyrinth barrier
782 that plays an essential role in the barrier integrity. PLoS One. 2011;6(1):e16547.
783 31. Uetsuka S, Ogata G, Nagamori S, Isozumi N, Nin F, Yoshida T, et al. Molecular
784 architecture of the stria vascularis membrane transport system, which is essential for
785 physiological functions of the mammalian cochlea. Eur J Neurosci. 2015;42(3):1984-
786 2002.
787 32. Sharlin DS, Visser TJ, Forrest D. Developmental and cell-specific expression of
788 thyroid hormone transporters in the mouse cochlea. Endocrinology. 2011;152(12):5053-
789 64.
790 33. Ando M, Takeuchi S. Immunological identification of an inward rectifier K+
791 channel (Kir4.1) in the intermediate cell (melanocyte) of the cochlear stria vascularis of
792 gerbils and rats. Cell Tissue Res. 1999;298(1):179-83.

34. Lek M, Karczewski KJ, Minikel EV, Samocha KE, Banks E, Fennell T, et al. Analysis of protein-coding genetic variation in 60,706 humans. Nature. 2016;536(7616):285-91.

35. Kowalczyk L, Ratera M, Paladino A, Bartoccioni P, Errasti-Murugarren E, Valencia E, et al. Molecular basis of substrate-induced permeation by an amino acid antiporter. Proc Natl Acad Sci U S A. 2011;108(10):3935-40.

36. Rosell A, Meury M, Alvarez-Marimon E, Costa M, Perez-Cano L, Zorzano A, et al. Structural bases for the interaction and stabilization of the human amino acid transporter LAT2 with its ancillary protein 4F2hc. Proc Natl Acad Sci U S A. 2014;111(8):2966-71.

37. Krishnamurthy H, Gouaux E. X-ray structures of LeuT in substrate-free outward-open and apo inward-open states. Nature. 2012;481(7382):469-74.

38. Noben-Trauth K, Zheng QY, Johnson KR. Association of cadherin 23 with polygenic inheritance and genetic modification of sensorineural hearing loss. Nat Genet. 2003;35(1):21-3.

39. Mazelova J, Popelar J, Syka J. Auditory function in presbycusis: peripheral vs. central changes. Exp Gerontol. 2003;38(1-2):87-94.

40. Xue Y, Mezzavilla M, Haber M, McCarthy S, Chen Y, Narasimhan V, et al. Enrichment of low-frequency functional variants revealed by whole-genome sequencing of multiple isolated European populations. Nat Commun. 2017;8:15927.

41. Minowa O, Ikeda K, Sugitani Y, Oshima T, Nakai S, Katori Y, et al. Altered cochlear fibrocytes in a mouse model of DFN3 nonsyndromic deafness. Science. 1999;285(5432):1408-11.

42. Wu T, Marcus DC. Age-related changes in cochlear endolymphatic potassium and potential in CD-1 and CBA/CaJ mice. J Assoc Res Otolaryngol. 2003;4(3):353-62.

43. Kikuchi T, Kimura RS, Paul DL, Takasaka T, Adams JC. Gap junction systems in the mammalian cochlea. Brain Res Brain Res Rev. 2000;32(1):163-6.

44. Teubner B, Michel V, Pesch J, Lautermann J, Cohen-Salmon M, Sohl G, et al. Connexin30 (Gjb6)-deficiency causes severe hearing impairment and lack of endocochlear potential. Hum Mol Genet. 2003;12(1):13-21.

45. Boettger T, Rust MB, Maier H, Seidenbecher T, Schweizer M, Keating DJ, et al. Loss of K-Cl co-transporter KCC3 causes deafness, neurodegeneration and reduced seizure threshold. EMBO J. 2003;22(20):5422-34.

46. Delprat B, Ruel J, Guitton MJ, Hamard G, Lenoir M, Pujol R, et al. Deafness and cochlear fibrocyte alterations in mice deficient for the inner ear protein otospiralin. Mol Cell Biol. 2005;25(2):847-53.

47. Trowe MO, Maier H, Schweizer M, Kispert A. Deafness in mice lacking the T-box transcription factor Tbx18 in otic fibrocytes. Development. 2008;135(9):1725-34.

48. Song MH, Choi SY, Wu L, Oh SK, Lee HK, Lee DJ, et al. Pou3f4 deficiency causes defects in otic fibrocytes and stria vascularis by different mechanisms. Biochem Biophys Res Commun. 2011;404(1):528-33.

49. Peter A. Santi PM. Cochlear Anatomy and Central Auditory Pathways. Cummings 2001. p. Chapter 140.

50. Wangemann P. Supporting sensory transduction: cochlear fluid homeostasis and the endocochlear potential. J Physiol. 2006;576(Pt 1):11-21.

838 51. Couloigner V, Sterkers O, Ferrary E. What's new in ion transports in the cochlea?
839 Pflugers Arch. 2006;453(1):11-22.
840 52. de Iriarte Rodriguez R, Magarinos M, Pfeiffer V, Rapp UR, Varela-Nieto I. C-Raf
841 deficiency leads to hearing loss and increased noise susceptibility. Cell Mol Life Sci.
842 2015;72(20):3983-98.
843 53. Everett LA, Belyantseva IA, Noben-Trauth K, Cantos R, Chen A, Thakkar SI, et
844 al. Targeted disruption of mouse Pds provides insight about the inner-ear defects
845 encountered in Pendred syndrome. Hum Mol Genet. 2001;10(2):153-61.
846 54. Camarero G, Avendano C, Fernandez-Moreno C, Villar A, Contreras J, de Pablo
847 F, et al. Delayed inner ear maturation and neuronal loss in postnatal Igf-1-deficient
848 mice. J Neurosci. 2001;21(19):7630-41.
849 55. Stankovic K, Rio C, Xia A, Sugawara M, Adams JC, Liberman MC, et al. Survival
850 of adult spiral ganglion neurons requires erbB receptor signaling in the inner ear. J
851 Neurosci. 2004;24(40):8651-61.
852 56. Sugawara M, Murtie JC, Stankovic KM, Liberman MC, Corfas G. Dynamic
853 patterns of neurotrophin 3 expression in the postnatal mouse inner ear. J Comp Neurol.
854 2007;501(1):30-7.
855 57. Zilberstein Y, Liberman MC, Corfas G. Inner hair cells are not required for
856 survival of spiral ganglion neurons in the adult cochlea. J Neurosci. 2012;32(2):405-10.
857 58. Efeyan A, Comb WC, Sabatini DM. Nutrient-sensing mechanisms and pathways.
858 Nature. 2015;517(7534):302-10.
859 59. Someya S, Prolla TA. Mitochondrial oxidative damage and apoptosis in age-
860 related hearing loss. Mech Ageing Dev. 2010;131(7-8):480-6.

861 60. Someya S, Tanokura M, Weindruch R, Prolla TA, Yamasoba T. Effects of caloric
862 restriction on age-related hearing loss in rodents and rhesus monkeys. Curr Aging Sci.
863 2010;3(1):20-5.
864 61. Bao J, Ohlemiller KK. Age-related loss of spiral ganglion neurons. Hear Res.
865 2010;264(1-2):93-7.
866 62. BioGPS [Internet]. 2001.
867 63. Zevenbergen C, Meima ME, Lima de Souza EC, Peeters RP, Kinne A, Krause G,
868 et al. Transport of Iodothyronines by Human L-Type Amino Acid Transporters.
869 Endocrinology. 2015;156(11):4345-55.
870 64. Hinz KM, Neef D, Rutz C, Furkert J, Kohrle J, Schulein R, et al. Molecular
871 features of the L-type amino acid transporter 2 determine different import and export
872 profiles for thyroid hormones and amino acids. Mol Cell Endocrinol. 2017.
873 65. Gomes P, Soares-da-Silva P. Na+-independent transporters, LAT-2 and b0,+,
874 exchange L-DOPA with neutral and basic amino acids in two clonal renal cell lines. J
875 Membr Biol. 2002;186(2):63-80.
876 66. Pinho MJ, Serrao MP, Gomes P, Hopfer U, Jose PA, Soares-da-Silva P. Over-
877 expression of renal LAT1 and LAT2 and enhanced L-DOPA uptake in SHR
878 immortalized renal proximal tubular cells. Kidney Int. 2004;66(1):216-26.
879 67. Peeters RP, Ng L, Ma M, Forrest D. The timecourse of apoptotic cell death
880 during postnatal remodeling of the mouse cochlea and its premature onset by
881 triiodothyronine (T3). Mol Cell Endocrinol. 2015;407:1-8.

882 68. Nunez B, Martinez de Mena R, Obregon MJ, Font-Llitjos M, Nunes V, Palacin M,
883 et al. Cerebral cortex hyperthyroidism of newborn mct8-deficient mice transiently
884 suppressed by lat2 inactivation. PLoS One. 2014;9(5):e96915.
885 69. Cediel R, Riquelme R, Contreras J, Diaz A, Varela-Nieto I. Sensorineural hearing
886 loss in insulin-like growth factor I-null mice: a new model of human deafness. Eur J
887 Neurosci. 2006;23(2):587-90.
888 70. Riquelme R, Cediel R, Contreras J, la Rosa Lourdes RD, Murillo-Cuesta S,
889 Hernandez-Sanchez C, et al. A comparative study of age-related hearing loss in wild
890 type and insulin-like growth factor I deficient mice. Front Neuroanat. 2010;4:27.
891 71. Murillo-Cuesta S, Camarero G, Gonzalez-Rodriguez A, De La Rosa LR, Burks
892 DJ, Avendano C, et al. Insulin receptor substrate 2 (IRS2)-deficient mice show
893 sensorineural hearing loss that is delayed by concomitant protein tyrosine phosphatase
894 1B (PTP1B) loss of function. Mol Med. 2012;18:260-9.
895 72. Sanchez-Calderon H, Rodriguez-de la Rosa L, Milo M, Pichel JG, Holley M,
896 Varela-Nieto I. RNA microarray analysis in prenatal mouse cochlea reveals novel IGF-I
897 target genes: implication of MEF2 and FOXM1 transcription factors. PLoS One.
898 2010;5(1):e8699.
899 73. de Iriarte Rodriguez R, Pulido S, Rodriguez-de la Rosa L, Magarinos M, Varela-
900 Nieto I. Age-regulated function of autophagy in the mouse inner ear. Hear Res.
901 2015;330(Pt A):39-50.
902 74. Esko T, Mezzavilla M, Nelis M, Borel C, Debniak T, Jakkula E, et al. Genetic
903 characterization of northeastern Italian population isolates in the context of broader
904 European genetic diversity. Eur J Hum Genet. 2013;21(6):659-65.

75. Timpson NJ, Walter K, Min JL, Tachmazidou I, Malerba G, Shin SY, et al. A rare variant in APOC3 is associated with plasma triglyceride and VLDL levels in Europeans. Nat Commun. 2014;5:4871.

76. Wang K, Li M, Hakonarson H. ANNOVAR: functional annotation of genetic variants from high-throughput sequencing data. Nucleic Acids Res. 2010;38(16):e164.

77. Costa M, Rosell A, Alvarez-Marimon E, Zorzano A, Fotiadis D, Palacin M. Expression of human heteromeric amino acid transporters in the yeast Pichia pastoris. Protein Expr Purif. 2013;87(1):35-40.

915 **Figures Legends and Tables**

916 **Figure 1. Hearing phenotype of C57BL6/J-129Sv *Slc7a8* knockout mice. (A)**
917 Representative image of Western bloting of total membranes from kidney, brain and
918 intestine of wild type (+/+) and *Slc7a8* knock out (-/-) mice in the absence (-) or
919 presence (+) of 100 mM dithiothreitol reducing agent (DTT) of 3 independent biological
920 samples for both sex (male and female). Protein (50 µg) were loaded in 7% acrylamide
921 SDS-PAGE gel. Molecular mass standard (KDa) are indicated. Red arrows point
922 SLC7A8/CD98hc heterodimer band as well as the light subunit SLC7A8. Upper panel:
923 Rabbit anti-SLC7A8. Bottom panel: Mouse anti-βactin. **(B)** Pre-Pulse Inhibition of the
924 acoustic startle response (PPI). Mean and SEM are represented. Pulse: 120 dB single
925 pulse. Pre-pulse inhibition test: six different pre-pulse intensities (70 to 90 dB) in pseudo
926 random order with 15 second inter-trial intervals. Wild type (white circles, n=19) and
927 *Slc7a8* $^{-/-}$ (blue circles, n=15) from 4- to 7-month-old are represented. Significant
928 differences were determined using paired Student's t-test, *** p<0.001 **(C-F)** Hearing
929 phenotype in wild type (*Slc7a8*$^{+/+}$, white, n=11), heterozygous (*Slc7a8*$^{+/-}$, green, n=12)
930 and knockout (*Slc7a8*$^{-/-}$, blue, n=14) mice, grouped by age (4-6 and 7-13 month old).
931 (C,D) Auditory Brainstem Response (ABR) threshold in response to click, expressed as
932 mean ± standard error (C), individual value (scatter plot, D) and median (boxplot, D).
933 The significance of the differences was evaluated using ANOVA test, *p<0.05, **p <
934 0.01 (*Slc7a8*$^{-/-}$ versus *Slc7a8*$^{+/+}$) and # p< 0.05 (*Slc7a8*$^{-/-}$ versus *Slc7a8*$^{+/-}$). E) Pie plot
935 showing the percentage of normal hearing (all thresholds < 45 dB SPL, white) mice and
936 mice with mild (at least 2 tone burst threshold > 45 dB SPL, orange) and severe (at
937 least 2 tone burst threshold > 60 dB SPL, red) hearing loss (HL), within each genotype

938 and age group. F) ABR thresholds in response to click and tone burst stimuli (8, 16, 24,
939 32 and 40 kHz) in mice from three genotypes separated by age group and hearing
940 phenotype (normal hearing or hearing loss). Significant differences were determined
941 using ANOVA test, *$p<0.05$, **$p < 0.01$, *** $p<0.001$ (hearing impaired *Slc7a8*$^{-/-}$ versus
942 normal hearing *Slc7a8*$^{+/+}$) and # $p< 0.05$ (hearing impaired *Slc7a8*$^{-/-}$ versus *Slc7a8*$^{+/-}$).
943

944 **Figure 2. <u>Immunolocalization of SLC7A8 in the mouse cochlea.</u> (A)** Representative
945 photomicrographs of cryosections of the base of the cochlea showing immunodetection
946 for SLC7A8 (green) and s100 (red); and staining for DAPI (blue) or phalloidin (white) of
947 wild type (upper row) and *Slc7a8*$^{-/-}$ mice (lower row). Scale bar, 100 µm. **(B)** On the left
948 overlay image of a wild type section indicating cochlea areas. Scale bar, 100 µm. On
949 the right schematic drawing of the adult scala media adapted from (72). BC, border
950 cells; CC, Claudius's cells; DC, Deiter's cells; HC, Hensen's cells; IC, intermediate cells;
951 IHC, inner hair cells; IPC, inner phalangeal cells; Li, spiral limbus; MB, Basilar
952 Membrane; OHC, outer hair cells; PC, pillar cells; RM, Reisner's membrane; SG, spiral
953 ganglion; SL, spiral ligament; SV, stria vascularis; TM, tectorial membrane. **(C)**
954 Quantification of SLC7A8 expression. Intensity of SLC7A8 immunofluorescence was
955 normalized per mm^2. Mean ± SEM from quadruplicates for each section, taken from
956 apex, middle and basal cochlear turns of 4 wild type (black), 3 *Slc7a8*$^{+/-}$ (green) and 4
957 *Slc7a8*$^{-/-}$ (blue) young (4- to 7-month old) mice. Open and closed circles represent
958 individual mice from C57BL6/J-129Sv or C57BL6/J backgrounds, respectevely.
959 Unpaired Student's t-test statistical analysis, p-values: *, ≤ 0.05; **, ≤ 0.01 and ***, ≤
960 0.001. **(D)** Quantification of SLC7A8 protein expression in the apex, middle and basal
961 cochlear turns normalized per nuclei of young (2 month-old) (open bars) and old (12
962 month-old) (black bars) wild type CBA mice. Data (mean ± SEM) were obtained from
963 four cochlear sections obtained from 3 mice per group. Unpaired Student's t-test
964 statistical analysis, p-value: *, ≤ 0.05.
965

966 **Figure 3. <u>Cytoarchitecture of the *Slc7a8*$^{-/-}$ mouse cochlea.</u> (A)** Hematoxylin
967 andEosin staining of the base of the cochlea. Representative photomicrographs taken
968 from paraffin sections of wild type and hipoacusic *Slc7a8*$^{-/-}$ mice. OC, Organ of Corti;
969 SG, spiral ganglia region; and SL, spiral ligament. * indicates loss of hair cells in the
970 organ of Corti (first column), loss of neurons in the spiral ganglia (second column) and
971 lower nuclei density in the spiral ligament (third column). Scale bar 100 μm. **(B)**
972 Quantification of the number of neurons in the spiral ganglia (SG) in the basal turns of
973 the cochlea. Y axis represents the mean nuclei quantification of 5 to 10 areas in SG. **(C)**
974 Quantification of the number of nuclei in the spiral ligament (SL) of the basal turns of the
975 cochlea by immunofluorescence using DAPI staining. For each sample, 12 overlaps of
976 Z-stacks areas were used to quantify number of nuclei. Unpaired Student's t-test
977 statistical analysis: **, $p \leq 0.01$ **(A to C)** 4 wild type (black), 3 *Slc7a8*$^{+/-}$ (green) and 4
978 *Slc7a8*$^{-/-}$ (blue) mice at 4-7-month old are represented. Circles represent the average of
979 the quadruplicate analysis performed in each mouse of C57BL6/J-129Sv (open) and
980 C57BL6/J (filled) background. **(D)** Quantification of mRNA markers by RT-qPCR PCR.
981 Cochlear gene expression of *Slc26a5, Tbx18, Kcnq2* and *Kcnq3* in the cochlea at 3-
982 month old and 7- months wild type (white bars) and *Slc7a8*$^{-/-}$ (blue bars) C57BL6/J
983 mice. Expression levels, normalized with *Rplp0* gene expression, are represented as n-
984 fold relative to control group. Values are presented as mean±SEM of triplicates from
985 pool samples of 3 mice per condition. Unpaired Student's t-test statistical analysis, p-
986 values: * $p \leq 0.05$; ** $p \leq 0.01$; *** $p \leq 0.001$.
987

988 **Figure 4. <u>Immunofluorescence of cochlear markers in the *Slc7a8*$^{-/-}$ mouse.</u> (A)**
989 Representative photomicrographs of cryosections (10 μm) from the basal turn of the
990 cochlea from wild type (1 and 4), *Slc7a8*$^{+/-}$ (2 and 5) and *Slc7a8*$^{-/-}$ (3 and 6) mice
991 labelled for Kir4.1 (green), phalloidin (red) and DAPI (blue) (1 to 3), or for s100 (red),
992 phalloidin (cyan) and DAPI (blue) (4 to 6). Scale bar, 100 μm. **(B, C** and **D)** Graph
993 representing the quantification of Kir4.1, s100 and phalloidin (Pha) labelling intensity in
994 the basal turn of the cochlea. Means ± SEM, normalized per mm^2 of 4 wild type (black
995 bars), 3 *Slc7a8*$^{+/-}$ (green bars) and 4 *Slc7a8*$^{-/-}$ (blue bars) young (4-7-month old) mice
996 are represented. Individual circles represent the average of the quadruplicate analysis
997 of sections from each mice of either C57BL6/J-129Sv (open) or C57BL6/J (filled)
998 backgrounds. Unpaired Student's t-test statistical analysis, p-value: *, ≤ 0.05.
999

1000 **Figure 5. *In vitro* characterization of SLC7A8 mutants. (A)** Panel showing
1001 representative images of immunofluorescence of wild type and the indicated SLC7A8
1002 mutants overexpressed in HeLa cells. Overlay of SLC7A8 (green), wheat germ
1003 agglutinin (WGA, membrane marker) (red) and the nuclear marker DAPI (blue) labeling.
1004 All SLC7A8 variants, except V460E, reached the plasma membrane. **(B)** Alanine (Ala)
1005 and tyrosine (Tyr) transport activity of human SLC7A8 wild type (WT) and mutants in
1006 transfected HeLa cells. SLC7A8 transport activity, corrected by SLC7A8-GFP
1007 expression, is presented as percentage of wild type SLC7A8 transport activity. Data
1008 (mean ± SEM) corresponds to three independent experiments with quadruplicates.
1009 Mutants activity comparing with its respectively wild type transport unpaired Student's t-
1010 test statistical analysis is represented, p-values: *, ≤ 0.05; **, ≤ 0.01 and ***, ≤ 0.001.

1011
1012 **Table 1**. ***SLC7A8* Humans mutations found in ARHL and controls individuals.**

1013 ARHL (age-related hearing loss). The age (years) of the subject when the Audiogram was performed is indicated. Variant
1014 [CHR: position reference/alternate (dbSNP135rsID)]. Consequence [HGUS annotation (protein change)]. Code [short
1015 description of the alternate variant]. Frequency of the mutations: Esp6500siv2 (NHLBI Exome Sequencing Project), 1000g
1016 (1000 Genomes Project), Campion (The Allele Frequency Net Database) and ExAC (The Exome Aggregation
1017 Consortium).

Phenotype	Age	Sex	Chr. 14	Variant	Consequence	Code	Frequency				
							Esp6500siv2	1000g	Campion	ExAC	Studied Cohort
ARHL	75	Female	23597290	14:23597291 C / T	p.Val460Glu	V460E	NA	NA	0.0013	0.00002475	0.015
ARHL	57	Male	23598917	14:23598917 G / A	p.Thr402Met	T402M	NA	NA	0.0047	0.00002471	0.015
ARHL	75	Male	23608641	14:23608641 C / T (rs142951280)	p.Val302Ile	V302I	0.0005	NA	0.0047	0.0004613	0.015
ARHL	86	Female	23598870	14:23598869 C / T	p.Arg418His	R418C	0.0005	NA	0.002	0.00002477	0.015
control	50	Male	23652101	14:23652101 C / G (rs141772308)	p.Arg8Pro	R8P	0.0008	NA	0.0013	0.0008156	0.012
control	50	Male	23635621	14:23635621 C / T (rs139927895)	p.Ala94Thr	A94T	0.0012	0.002	0.0013	0.00202	0.012
control	90	Female	23612368	14:23612368 C / T (rs149245114)	p.Arg185Gln	R185L	NA	NA	0.002	0.00002471	0.012

1018

1019 **Table 2**. **Key Resources Table**

Reagent type (species) or resource	Designation	Source or reference	Identifiers	Additional information
antibody	SLC7A8 antibody	Custom made	NA	Anti-Rabbit peptide sequence: PIFKPTPVKDPDSEE QP WB: 1:1000, IHC: 1/5000 and IF:1/200
	s100	Sigma-Aldrich	Ref: S2532	IF: 1/1000
	Kir4.1	Merck Millipore	Ref: AB5818	IF: 1/200
	BA1	Abcam	Ref: ab5076	IF: 1/200
	Phalloidin	Thermo Fisher Scientific	Ref: A22287	IF: 1/100
	Donkey anti-Goat Alexa Fluor 546	Thermo Fisher Scientific	Ref: A-11056	IF: 1/300
	Donkey anti-Rabbit Alexa Fluor 488	Thermo Fisher Scientific	Ref: A-21206	IF: 1/300
	Goat anti-Mouse Alexa Fluor 546	Thermo Fisher Scientific	Ref: A-11030	IF: 1/300
	Goat anti-Rabbit Alexa Fluor 488	Thermo Fisher Scientific	Ref: A-11034	IF: 1/300
	WGA	Thermo Fisher Scientific	Ref: W21405	labeled with Texas-Red IF: 1mg/mL
	anti-Strep Tag GT517	Abcam	Ref: ab184224	IF: 1/100
	goat-anti-mouse-	Abcam	Ref: ab6785	IF: 1/300

	FITC			
Behavior	Rotarod	Panlab	Ref:LE8500	
	Treadmill	Panlab	E8710MTS	
	Morris water maze	Panlab	SMART camera	circular tank (150 cm diameter, 100 cm high)
	PPI	Panlab	LE116	
	Restrain stressor	Lab Research	Ref:G05	
	ABR	Tucker Davis Technologies TDT	System 3 Evoked	
Mouse	C57BL6/J wild type	Harlam	Ref: 057	C57BL/6JOlaHsd
	C57BL6/J wild type	Jackson laboratory	Ref: 000664/Black	
	Slc7a8-/- chimera	Genoway	Customized Model Development	Strategy Figure 1-figure supplement 1
Cell Line	HeLa	Sigma Aldrich,	Ref: 93021013	
chemical compound, drug	DTT dithiothreitol	SigmaAldrich	Ref:D9779	
	L- [^{3}H]-labeled alanine	Perkin Elmer	Ref: NET348250UC	1 µCi/ml
	[3H]-tyrosine	Perkin Elmer	Ref: NET127250UC	1 µCi/ml
commercial assay or kit	Pierce BCA Protein Assay Kit	Thermo Scientific	Ref:23225	
	ECL	GE Healthcare	Ref:RPN2232	
	Corticosterone EIA kit	Enzo	Ref:ADI900097	
	A+B conjugate	Vectastain,	Ref: ABC kit	
	Rneasy	Qiagen	Ref: 74104	

	High Capacity cDNA Reverse Transcription Kit	Applied Biosystems	Ref: 4368813	
	TaqMan Gene Expression Assay	Applied Biosystems	potassium voltage-gated channel subfamily Q member 2 (*Kcnq2*) Mm00440080_m1; potassium voltage-gated channel subfamily Q member 3 (*Kcnq3*) Mm00548884_m1; potassium voltage-gated channel subfamily Q member 5 (*Kcnq5*) Mm01226041_m1; prestin (*Slc26a5*) Mm00446145_m1; T-box transcription factor TBX18 (*Tbx18*) Mm00470177_m1; interleukin 1 beta (*Il1b)* Mm00434228m1; interleukin 6 (*Il6)* Mm00446190m1; solute carrier family 7 (cationic amino acid transporter, y+ system), member 8 (*Slc7a8)* Mm01318971m1	
	QuikChange site-directed mutagenesis kit	Stratagene	Ref: 200524	
gene (human)	*SLC7A8*	NCBI	NM_012244.3	Protein NP_036376.2 (535AA)
	Slc7a8	NCBI	NM_016972.2	Protein NP_058668.1 (531AA)
sequence-based reagent	whole genome sequence	Illumina	HiSeq 2000	Data coverage was ranging from 4 to 10X
	Sanger sequencing	Life Technologies	3500 Dx Genetic Analyzer	
	BigDye	Life Technologies	ABI PRISM 3.1 Big Dye terminator	
software, algorithm	BioSig®	Tucker Davis Technologies TDT	NA	

	Graph Pad Software	GraphPad Software, Inc	Prism 4	https://www.graphpad.com/scientific-software/prism/
	SeqMan Pro software	DNAstar	https://www.dnastar.com/t-seqmanpro.aspx	sequencing assembly and analysis
	Annotations tools	ANNOVAR	http://annovar.openbioinformatics.org/en/latest/	functional annotation of genetic variants DOI:10.1093
	Genome Research	Bcftools	http://samtools.github.io/bcftools/	
	SPSS 23.0 statistic software package	IBM	NA	https://www.ibm.com/analytics/data-science/predictive-analytics/spss-statistical-software
transfected construct	Slc7a8 construct	Agilent	Catalog #212205	Resistances: Neomycin and thymidine kinase
	pcDNA3.1-StrepTag	ThermoFisher	Ref: V79020	fused SLC7A8 or SLC3A2

1020

Supplementary Figures

Figure 1-figure supplement 1. Scheme of *Slc7a8* knockout mouse generation. (A) Diagram of the homologous recombination in *Slc7a8* locus, the vector used to replace the coding region of the gene for a neomycin (Neo) resistance and the resulting recombinant locus. **(B)** Scheme of LAT2 protein, in gray deleted region in the *Slc7a8* $^{-/-}$ mouse and in red is represented the epitope which anti-SLC7A8 antibody was generated.

1029 **Figure 1-figure supplement 2. <u>SLC7A8 expression in mouse brain</u>. (A)** Wild type
1030 mouse brain immunohistochemistry against SLC7A8 in wild type 4- to 7-months of age
1031 in mixed C57BL6/J-129Sv genetic background mice. Arrow is pointing SLC7A8
1032 expression in cell membranes. 1: Cerebral cortex, SLC7A8 expression is localized to
1033 apical dendrites and synaptic area. 2 and 3: Preoptic Area. SLC7A8 expression in
1034 fibers. 4: Hypophysis. 5: Brain blood vessel. 6: Subfornical organ. 7: Choroid plexus. **(B)**
1035 Representative Image from the scan (Nanozoomer, Hamamatsu Photon) of the whole
1036 cochlea immunofluorescence. SLC7A8 (green), phalloidin (red) and DAPI (blue)
1037 markers of wild type (upper row) and *Slc7a8*$^{-/-}$ (bottom row) adult mice (4- to 7-months
1038 of age in mixed C57BL6/J-129Sv genetic background) are represented. The selected
1039 spiral ganglion areas (orange square) are magnified on the right, where white arrow
1040 points SLC7A8 signal in the spiral ganglia neurons that is specific as it fades completely
1041 in the *Slc7a8*$^{-/-}$ mice. Scale bar 100 μm.
1042

1043 **Figure 1-figure supplement 3. <u>Behavior phenotype</u>. (A to G)** Behavior tests data
1044 (mean ± SEM) of wild type (open circles) and *Slc7a8*$^{-/-}$ (black circles) mice of 4- to 7-
1045 months of age in mixed C57BL6/J-129Sv genetic background. **(A)** Latency to fall off the
1046 rod in the rotarod test at increasing fixed rotating speed (rpm) (n = 16 wild type and 14
1047 Slc7a8$^{-/-}$); **(B** and **C)** Time of exposure to shock in the treadmill test. Higher values
1048 indicate poorer performance (n = 8 wild type and 8 Slc7a8$^{-/-}$). **(D** to **F)** Morris Water
1049 Maze (MWM) test of 5 wild type and 8 *Slc7a8*$^{-/-}$ mice. **(G)** Represents Rotarod
1050 Acceleration Time from 4 to 40rpm in 60 sec. Unpaired Student's t-test statistical
1051 analysis, p-value: *, ≤ 0.05. **(H)** Western blot against SLC7A8 of 50 µg of total
1052 membranes from hypophysis of wild type (+/+), *Slc7a8*$^{+/-}$ (+/-) and *Slc7a8*$^{-/-}$ (-/-) mice.
1053 Kidney sample from wild type mice was used as a positive control. Samples were
1054 loaded in 7% acrylamide SDS-PAGE gel in non-reducing conditions. SLC7A8/CD98hc
1055 heterodimers (120kDa) were detected. **(I)** Plasma corticosterone levels after acute
1056 stress. Data (mean ± SEM) from 4 wild type (open bars) and 5 *Slc7a8*$^{-/-}$ mice (black
1057 bars) are represented. Basal: time 0, Stress: just after mice were exposed to a 15 min
1058 restraint stress and Recovery: 90 min after the stress.
1059

Figure 1-figure supplement 4. <u>ABR latencies and amplitudes of C57BL6/J-129Sv *Slc7a8* knockout mice</u>. (A) Representative ABR recordings in response to click at decreasing intensities from 90 to 10 dB SPL from wild type (*Slc7a8*$^{+/+}$, white, n=11), heterozygous (*Slc7a8*$^{+/-}$, green, n=12) and knockout (*Slc7a8*$^{-/-}$, blue, n=14) mice, grouped by age (4-6 and 7-13 month old). ABR waves I to IV are indicated and thresholds highlighted in bold. Detail of the first ms of the ABR recording in response to 70 dB SPL click showing the differences in the wave I latency and amplitude among genotypes (dashed lines). **(B-E)** Latency and amplitude of ABR waves, expressed as mean ± SE, in wild type (*Slc7a8*$^{+/+}$, white, n=14), heterozygous (*Slc7a8*$^{+/-}$, green, n=12) and knockout (*Slc7a8*$^{-/-}$, blue, n=11) separated by age group (4-6 and 7-13 month old) and hearing phenotype (normal hearing and hearing loss). **(B)** Latency-intensity curves for ABR wave I. **(C)** Interpeak latencies I-II, II-IV and I-IV in response to 70 dB SPL click. Significant differences were determined using ANOVA test, *$p<0.05$ (*Slc7a8*$^{-/-}$ versus *Slc7a8*$^{+/+}$ mice). **(D)** Amplitude-intensity curves for ABR wave I. **(E)** Amplitudes of ABR wave I, II and IV. Significant differences were determined using ANOVA test, #$p<0.05$ (hearing loss *Slc7a8*$^{-/-}$ vs normal hearing *Slc7a8*$^{+/-}$ mice).

1078 **Figure 1-figure supplement 5. Hearing phenotype of C57BL/6J *Slc7a8* knockout**
1079 **mice. (A, B)** Auditory Brainstem Response (ABR) thresholds in response to click stimuli
1080 in from wild type (*Slc7a8*$^{+/+}$, white, n=18), heterozygous (*Slc7a8*$^{+/-}$, green, n=5) and
1081 knockout (*Slc7a8*$^{-/-}$, blue, n=15) mice, grouped by age (1-3, 4-6 and 7-13 month-old)
1082 and expressed as mean ± standard error (A), individual value (scatter plot, B) and
1083 median (boxplot, B). The significance of the differences was evaluated using ANOVA
1084 test, *p<0.05 (*Slc7a8*$^{-/-}$, versus *Slc7a8*$^{+/+}$). (**C)** Auditory Brainstem Response (ABR)
1085 thresholds in response to click stimuli in from wild type (*Slc7a8*$^{+/+}$, white, n=18) and
1086 knockout (*Slc7a8*$^{-/-}$, blue, n=15) mice at 2, 3, 4 and 5 month life. **(D)** Pie chart showing
1087 the percentage of mice showing normal hearing (all thresholds < 45 dB SPL, white),
1088 mild hearing loss (at least 2 tone burst threshold > 45 dB SPL, orange) and severe (at
1089 least 2 tone burst threshold > 60 dB SPL, red) hearing loss (HL), within each genotype
1090 and age group. **(E)** ABR thresholds in response to click and tone burst stimuli (8, 16, 24,
1091 32 and 40 kHz) in mice from three genotypes separated by age group and hearing
1092 phenotype (normal hearing or hearing loss). Significant differences were determined
1093 using ANOVA test, **p < 0.01, *** p<0.001 (hearing impaired *Slc7a8*$^{-/-}$ versus *Slc7a8*$^{+/+}$).
1094

1095 **Figure 2-figure supplement 1. <u>Quantification of transcripts in the *Slc7a8*$^{-/-}$ mouse</u>**
1096 **<u>cochlea.</u> (A)** *Slc7a8* mRNA expression in cochlea at different ages in mice in
1097 MF1/129Sv genetic background. Expression levels, normalized by *Hrpt1* gene
1098 expression, are represented as n-fold relative to control group (1-2 month-old). Values
1099 are presented as mean ± SEM of triplicates from pooled sample of 3 mice per group.
1100 Unpaired Student's t-test statistical analysis (*: E18.5 versus other groups. ^: 1-2
1101 months versus other groups) p-values: *,^ $p \leq 0.05$; **,^^ $p \leq 0.01$; ***,^^^$p \leq 0.001$. **(B
1102 and C)** mRNA levels were determined by RT-qPCR in the cochlea of 3 wild type and 3
1103 *Slc7a8*$^{-/-}$ young (3-7-month old) C57BL6/J mice run in triplicates. Data (mean ± SEM)
1104 correspond to relative value normalized with *Rplp0* gene expression. Unpaired
1105 Student's t-test statistical analysis, p-values: *, ≤ 0.05, **, $^{\&\&} \leq 0.01$, ***, $^{\&\&\&} \leq 0.001$ and
1106 ****, $^{\&\&\&\&} \leq 0.0001$. (B) Potassium voltage-gated channel subfamily Q member 5
1107 (*Kcnq5*), (C) interleukin-1 (*Il1*) and interleukin-6 (*Il6*).
1108

1109 **Figure 2-figure supplement 2. Progression of hearing phenotype of C57BL/6J**
1110 ***Slc7a8* knockout mice**. **(A)** Longitudinal analysis of Auditory Brainstem Response
1111 (ABR) thresholds in response to click stimuli in wild type (*Slc7a8*$^{+/+}$, white, n=19),
1112 heterozygous (*Slc7a8*$^{+/-}$, green, n=13) and knockout (*Slc7a8*$^{-/-}$, blue, n=23) mice,
1113 through 2 to 5 months of age, and expressed as mean ± standard error. The
1114 significance of the differences was evaluated using ANOVA test, $p<0.05$ (*Slc7a8*$^{-/-}$
1115 versus Slc7a8$^{+/+}$ [*] or versus *Slc7a8*$^{+/-}$ [#]). **(B)** Pie chart showing the percentage of
1116 mice with normal hearing (all thresholds < 45 dB SPL, white), mild hearing loss (HL) (at
1117 least 2 tone burst threshold > 45 dB SPL, orange) and severe HL (at least 2 tone burst
1118 threshold > 60 dB SPL, red), within each genotype and age group.
1119

1120 **Figure 3-figure supplement 1. <u>Correlations of the cell numbers and cell type</u>**

1121 **<u>biomarkers with HL phenotype</u>. (A)** Pearson's correlation (CI 95%) between ABR

1122 threshold and Spiral Ganglia (SG) nuclei number with a p-value of 0.001 is represented.

1123 **(B-D)** Individual mouse representation of SG nuclei number (B), Intensity of Kir4.1

1124 marker (C) and number or fibrocytes in the spiral ligament (D) categorized by mouse

1125 phenotype: normal (open bars), mild (orange bars) and severe (red bars) hearing loss.

1126 Individual circles represent the average of the replicates for each analysis from wild type

1127 (black bars), *Slc7a8*$^{+/-}$ (green bars) and *Slc7a8*$^{-/-}$ (blue bars) adult mice (4-7-month old);

1128 either C57BL6/J-129Sv (open) or C57BL6/J (filled) backgrounds. Paired Student's t-test

1129 statistical analysis, p-value: *, ≤ 0.05 and **, ≤ 0.01.

1130

1131 **Figure 4-figure supplement 1. <u>Quantification of the intensity of cell type</u>**

1132 **<u>biomarkers in apical and middle cochlear regions</u>**. Quantification of

1133 immunofluorescence labeling normalized per mm^2 of Kir4.1 **(A)**, s100 **(B),** phalloidin

1134 (Pha) **(C)** and IBA1 **(D)** in apical, middle and basal turns cryosections of the cochlea.

1135 Mean ± SEM data were compiled from 3-4 wild type (black bars), 3 *Slc7a8*$^{+/-}$ (green

1136 bars) and 4 *Slc7a8*$^{-/-}$ (blue bars) adult (4-7-month old) mice. Individual circles represent

1137 the average of the quadruplicate analysis of sections from mice of either C57BL6/J-

1138 129Sv (open) or C57BL6/J (filled) backgrounds. Unpaired Student's t-test statistical

1139 analysis, p-value: *, ≤ 0.05.

1140

1141 **Figure 5-figure supplement 1. <u>Audiogram of patients with ARHL and localization</u>**
1142 **<u>of the mutations in SLC7A8 protein.</u> (A and B)** Graphs representing the pure-tone
1143 audiometry performed using standard audiometers in ARHL patients and controls
1144 carrying SLC7A8 mutations. The analysis of hearing functions was performed by
1145 determining the pure tone average of air conduction (PTA) at different frequencies:
1146 lower (0.125, 0.25 and 0.5 kHz), medium (1 and 2 kHz), and high (4, 8 kHz). Audiometry
1147 of the best hearing ear is shown for each individual. Salmon box indicates the inclusion
1148 criteria considered for ARHL phenotype. **(A)** ARHL cases (threshold > 40dB at PTA-H)
1149 and **(B)** Controls (threshold < 25dB at PTA-H). **(C-D)** Cartoon representation of the
1150 actual structural model of SLC7A8/CD98hc heterodimer. **(C)** The ectodomain of human
1151 CD98hc (gray) and human SLC7A8 (pale-green) in an outward-facing conformation are
1152 shown. The transmembrane (TM) domain of CD98hc is not shown because there is no
1153 structural information about its localization. Residues involved in sequence variants
1154 identified in patients with ARHL are highlighted (atoms represented by spheres). Atoms
1155 are colored according to: O (red), N (blue) and C-atoms depending on the residue
1156 (V302, pale-pink; T402, magenta; R418, gray and V460, slate-blue). The pale-yellow
1157 band is shown to visualize the insertion of SLC7A8 in the membrane. Residue R418 is
1158 located in the intracellular loop between TM domains 10 and 11, and residue V460 is
1159 located at the end of the TM domain 12, just before the intracellular C-terminus that is
1160 not depicted. **(D)** Top view close-up from outside the cell showing the localization of
1161 residues V302 and T402 respectively. To facilitate the view, the extracellular domain of
1162 CD98hc has been deleted. Unwound segments of TM domains 1 and 6 that interact
1163 with the α-amino-carboxyl end of the amino acid substrates are colored in blue and red

1164 respectively. Residue V302 is located in the extracellular loop 4 (EL4) (orange), which
1165 contains a double α helix structure that closes the substrate binding cavity in the inward-
1166 facing conformations. Residue T402 is located in TM domain 10 facing the substrate
1167 binding cavity.
1168

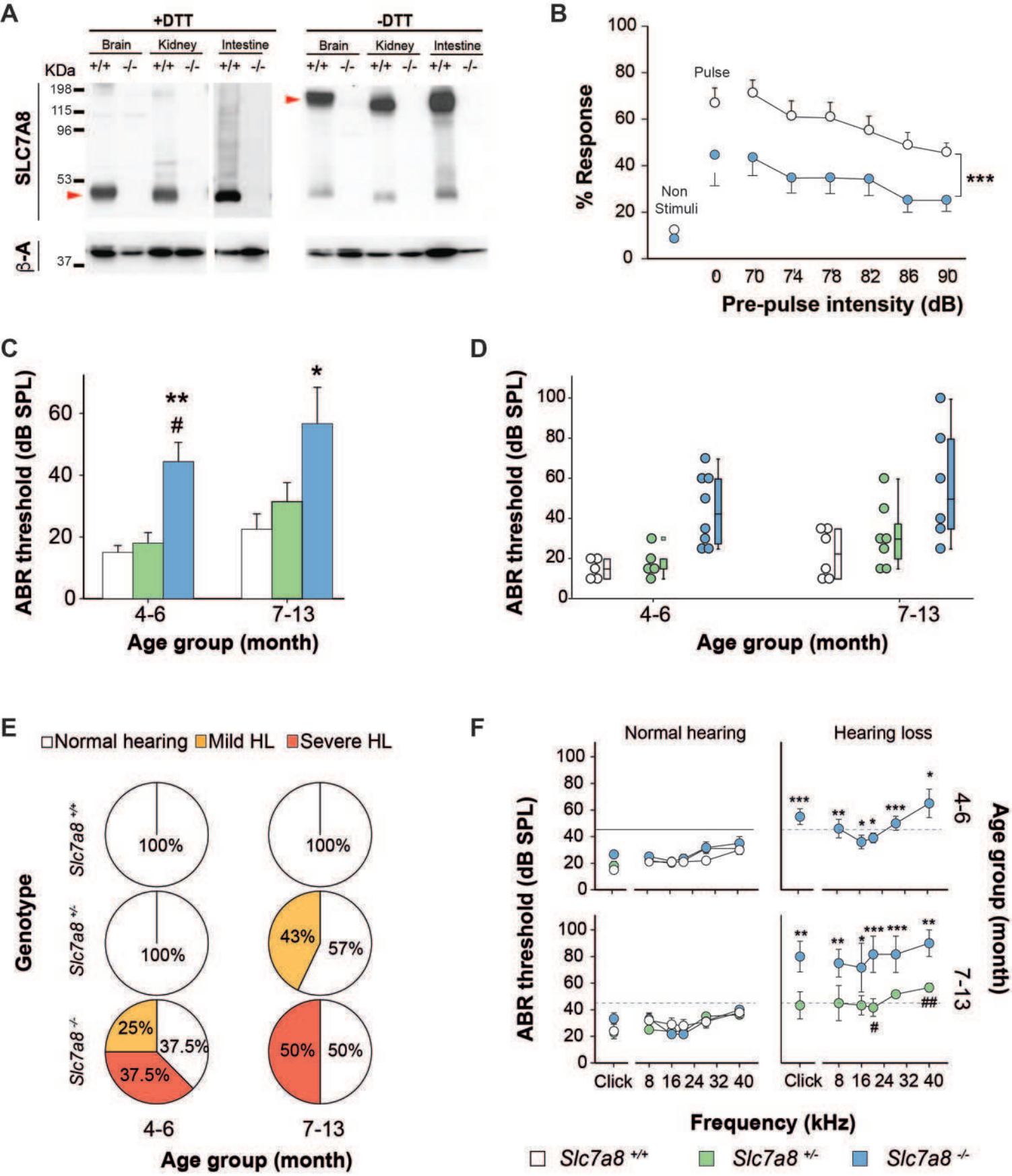
A
+DTT
-DTT
Brain
Kidney
Intestine
KDa
+/+ -/-
198
115
96
53
37
SLC7A8
β-A
B
% Response
Pulse
Non Stimuli
***
Pre-pulse intensity (dB)
C
ABR threshold (dB SPL)
**
#
*
4-6
7-13
Age group (month)
D
ABR threshold (dB SPL)
Age group (month)
E
Normal hearing
Mild HL
Severe HL
Genotype
Slc7a8 +/+
Slc7a8 +/-
Slc7a8 -/-
100%
43%
57%
25%
37.5%
50%
Age group (month)
F
Normal hearing
Hearing loss
ABR threshold (dB SPL)
Age group (month)
Click 8 16 24 32 40
Frequency (kHz)
Slc7a8 +/+
Slc7a8 +/-
Slc7a8 -/-

A

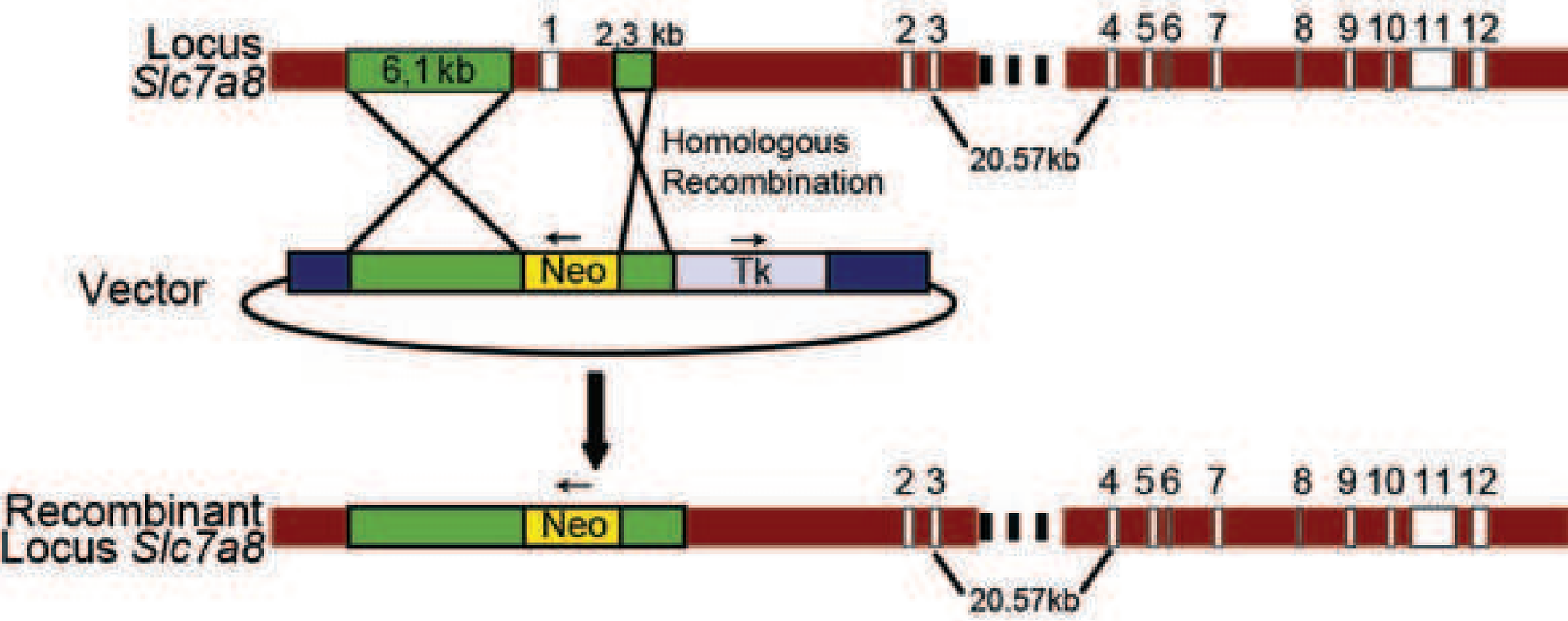
Locus
Slc7a8
6,1 kb
1
2,3 kb
2 3
4 5 6 7
8 9 10 11 12
Homologous
Recombination
20.57kb
Vector
Neo
Tk
Recombinant
Locus Slc7a8
Neo
2 3
4 5 6 7
8 9 10 11 12
20.57kb

B


I
II
III
IV
V
VI
VII
VIII
IX
X
XI
XII

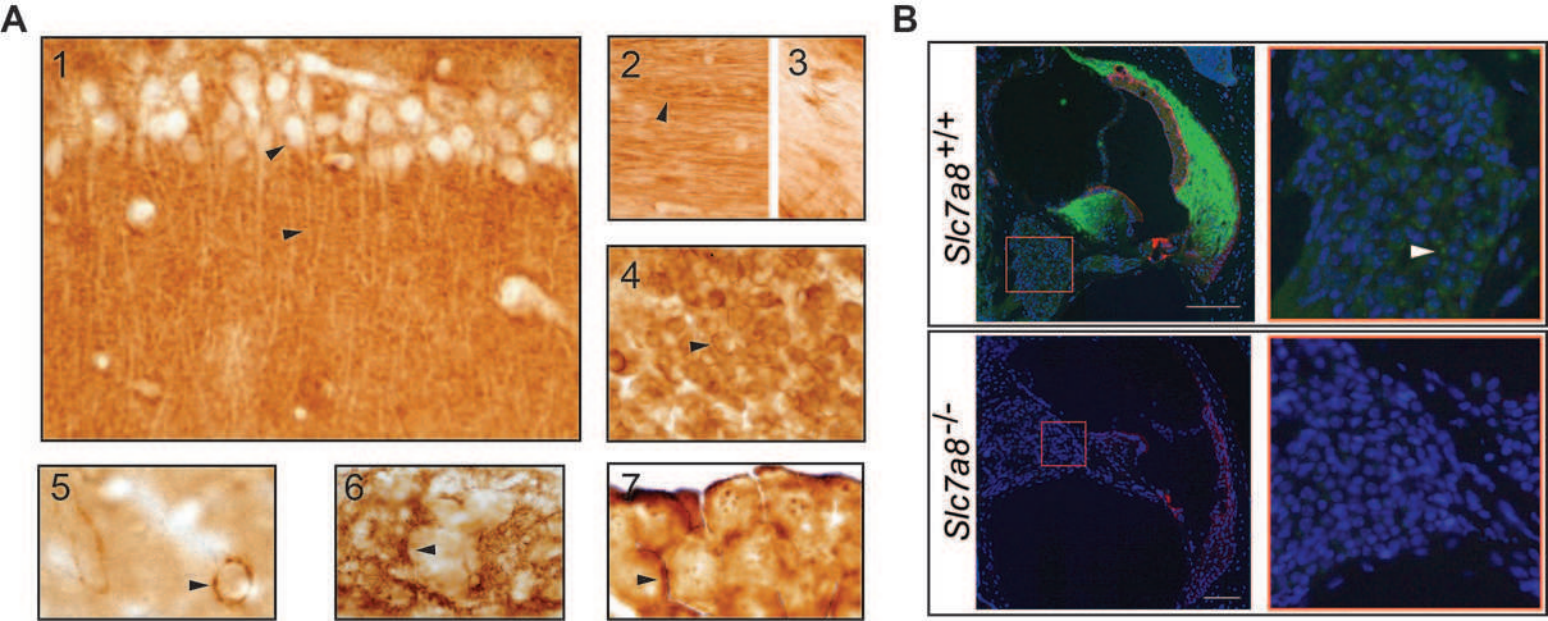
A
1
2
3
4
5
6
7
B
Slc7a8+/+
Slc7a8-/-

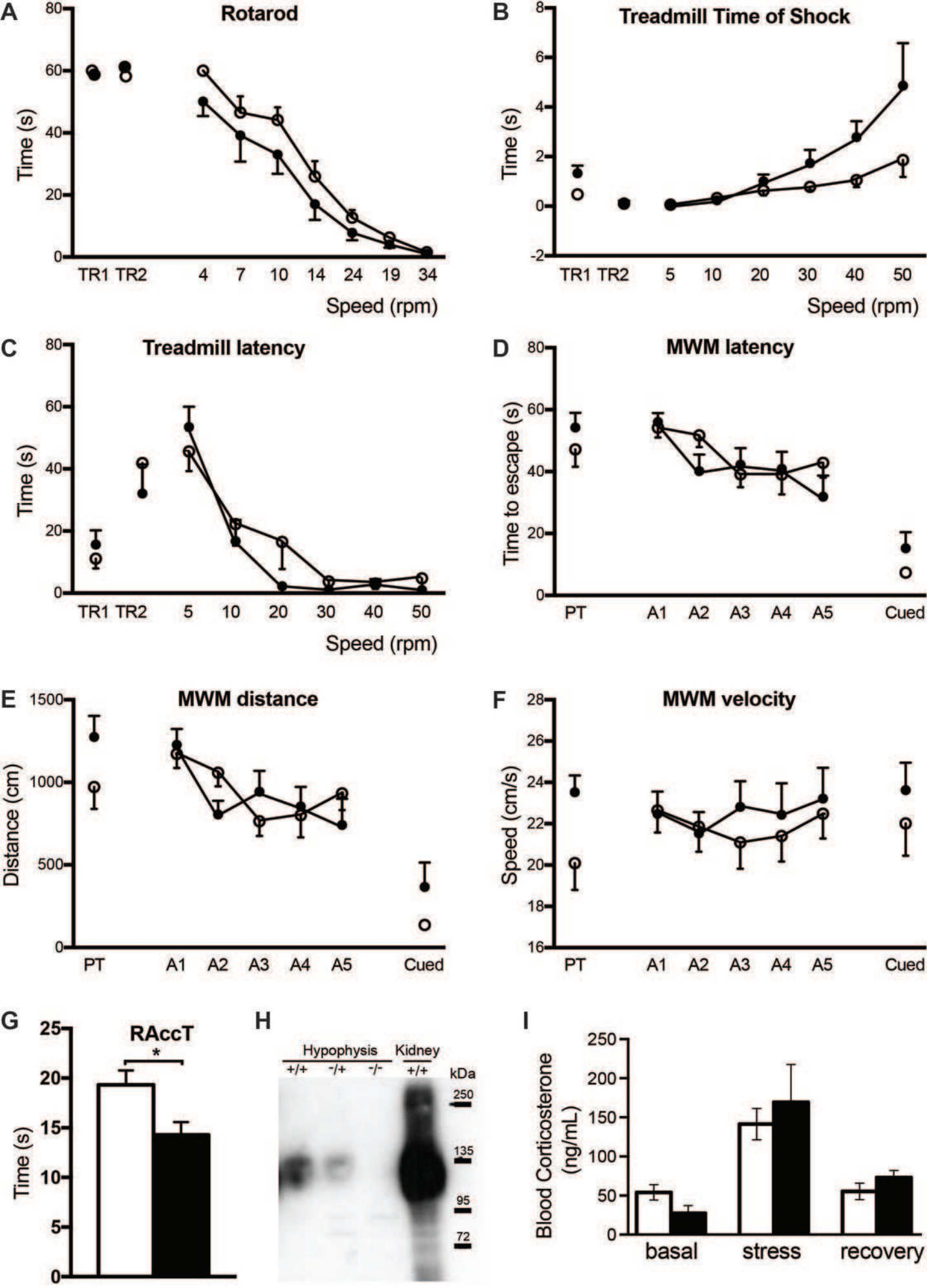
A
Rotarod
Time (s)
TR1 TR2 4 7 10 14 24 19 34
Speed (rpm)
B
Treadmill Time of Shock
Time (s)
TR1 TR2 5 10 20 30 40 50
Speed (rpm)
C
Treadmill latency
Time (s)
TR1 TR2 5 10 20 30 40 50
Speed (rpm)
D
MWM latency
Time to escape (s)
PT A1 A2 A3 A4 A5 Cued
E
MWM distance
Distance (cm)
PT A1 A2 A3 A4 A5 Cued
F
MWM velocity
Speed (cm/s)
PT A1 A2 A3 A4 A5 Cued
G
RAccT
*
Time (s)
H
Hypophysis
Kidney
+/+ -/+ -/- +/+
kDa
250
135
95
72
I
Blood Corticosterone (ng/mL)
basal
stress
recovery

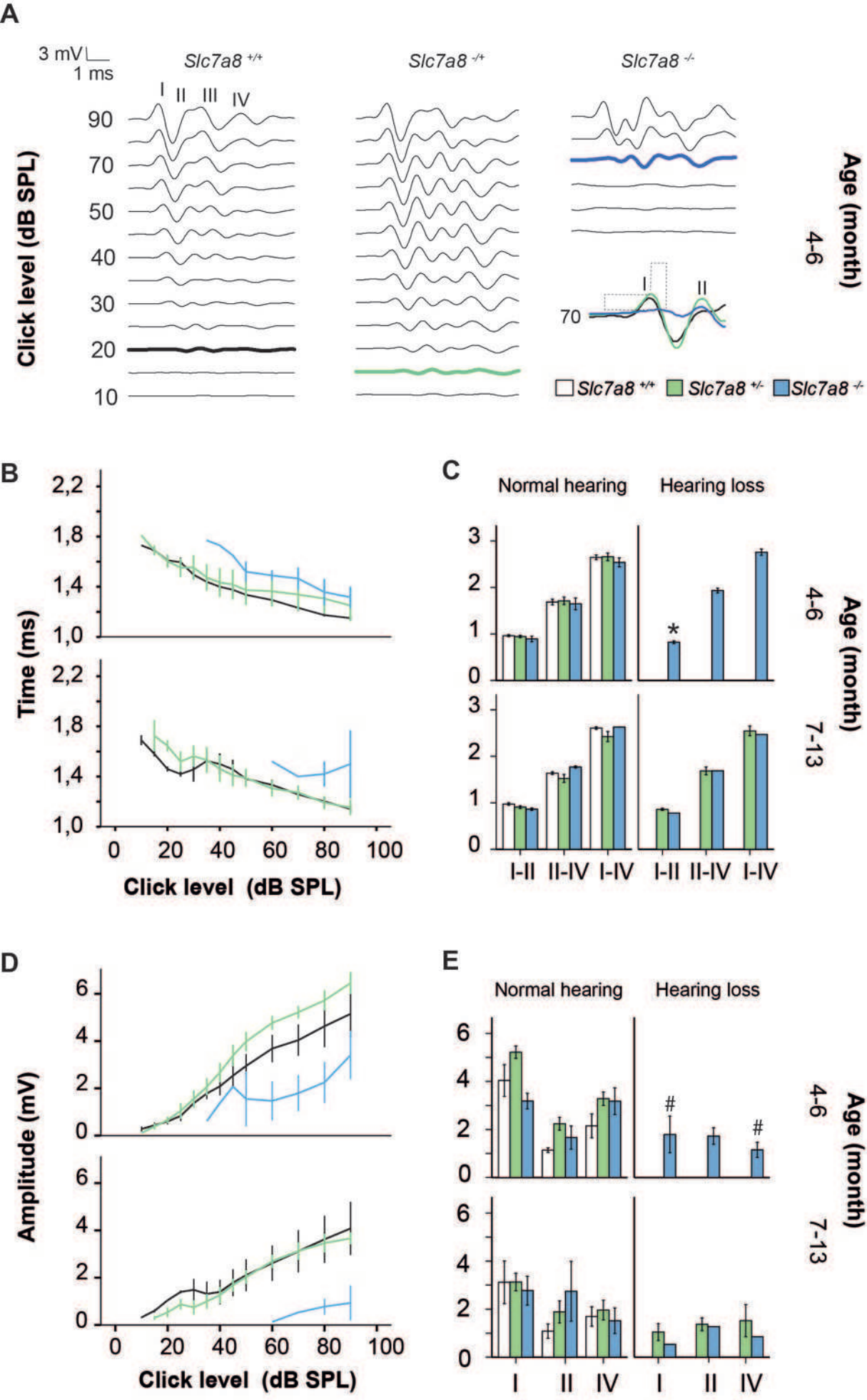
A
3 mV
1 ms
Slc7a8 +/+
Slc7a8 -/+
Slc7a8 -/-
I
II
III
IV
90
70
50
40
30
20
10
Click level (dB SPL)
Age (month)
4-6
70
Slc7a8 +/+
Slc7a8 +/-
Slc7a8 -/-
B
2,2
1,8
1,4
1,0
Time (ms)
0
20
40
60
80
100
Click level (dB SPL)
C
Normal hearing
Hearing loss
3
2
1
0
*
4-6
7-13
Age (month)
I-II
II-IV
I-IV
D
6
4
2
0
Amplitude (mV)
Click level (dB SPL)
E
#
I
II
IV

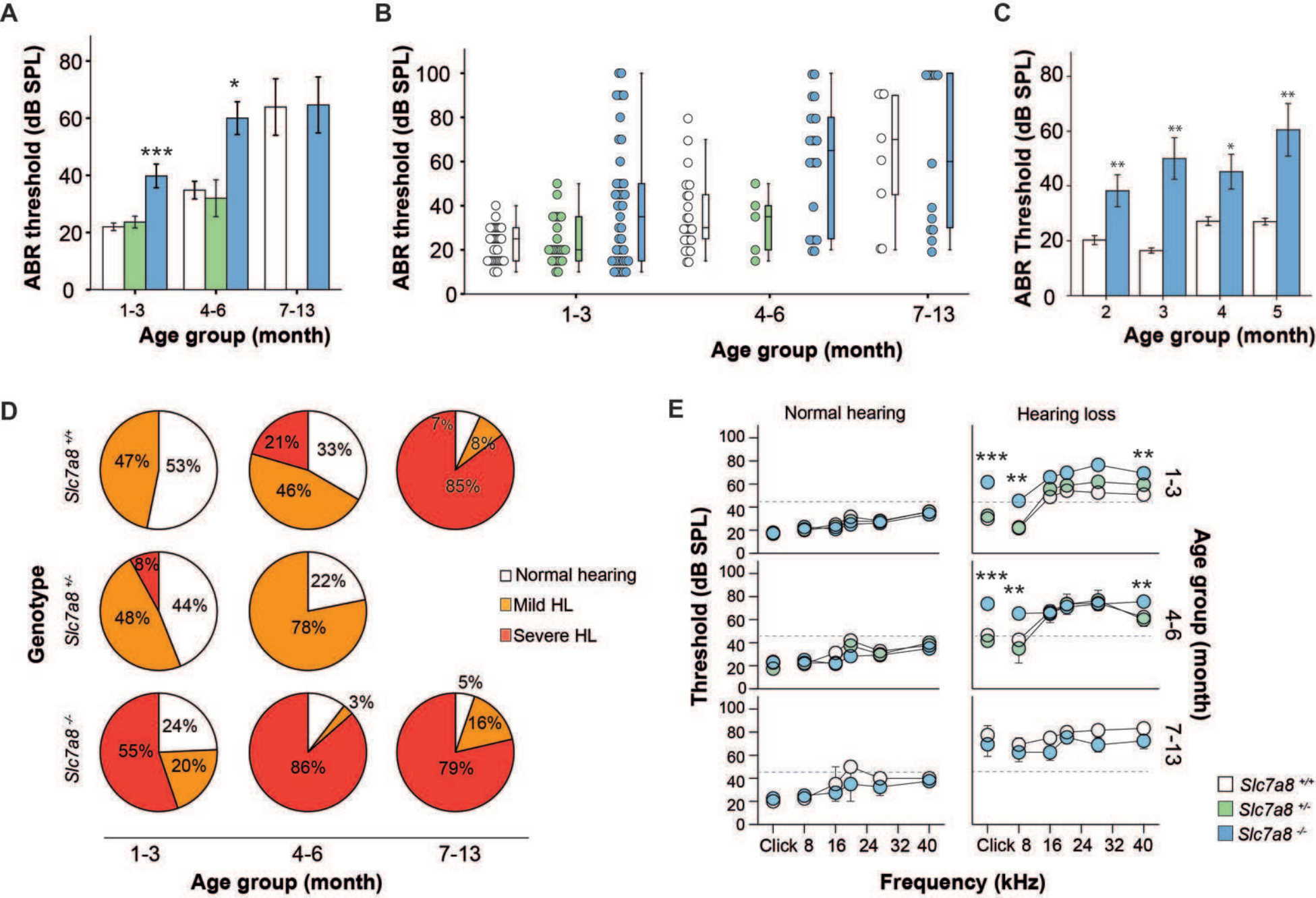
A
ABR threshold (dB SPL)
0
20
40
60
80
***
*
1-3
4-6
7-13
Age group (month)
B
ABR threshold (dB SPL)
0
20
40
60
80
100
1-3
4-6
7-13
Age group (month)
C
ABR Threshold (dB SPL)
0
20
40
60
80
**
**
*
**
2
3
4
5
Age group (month)
D
Genotype
Slc7a8 +/+
Slc7a8 +/-
Slc7a8 -/-
47%
53%
21%
33%
46%
7%
8%
85%
8%
48%
44%
22%
78%
24%
55%
20%
3%
86%
5%
16%
79%
Normal hearing
Mild HL
Severe HL
1-3
4-6
7-13
Age group (month)
E
Normal hearing
Hearing loss
Threshold (dB SPL)
0
20
40
60
80
100
***
**
***
**
**
**
1-3
4-6
7-13
Age group (month)
Click 8 16 24 32 40
Frequency (kHz)
Slc7a8 +/+
Slc7a8 +/-
Slc7a8 -/-

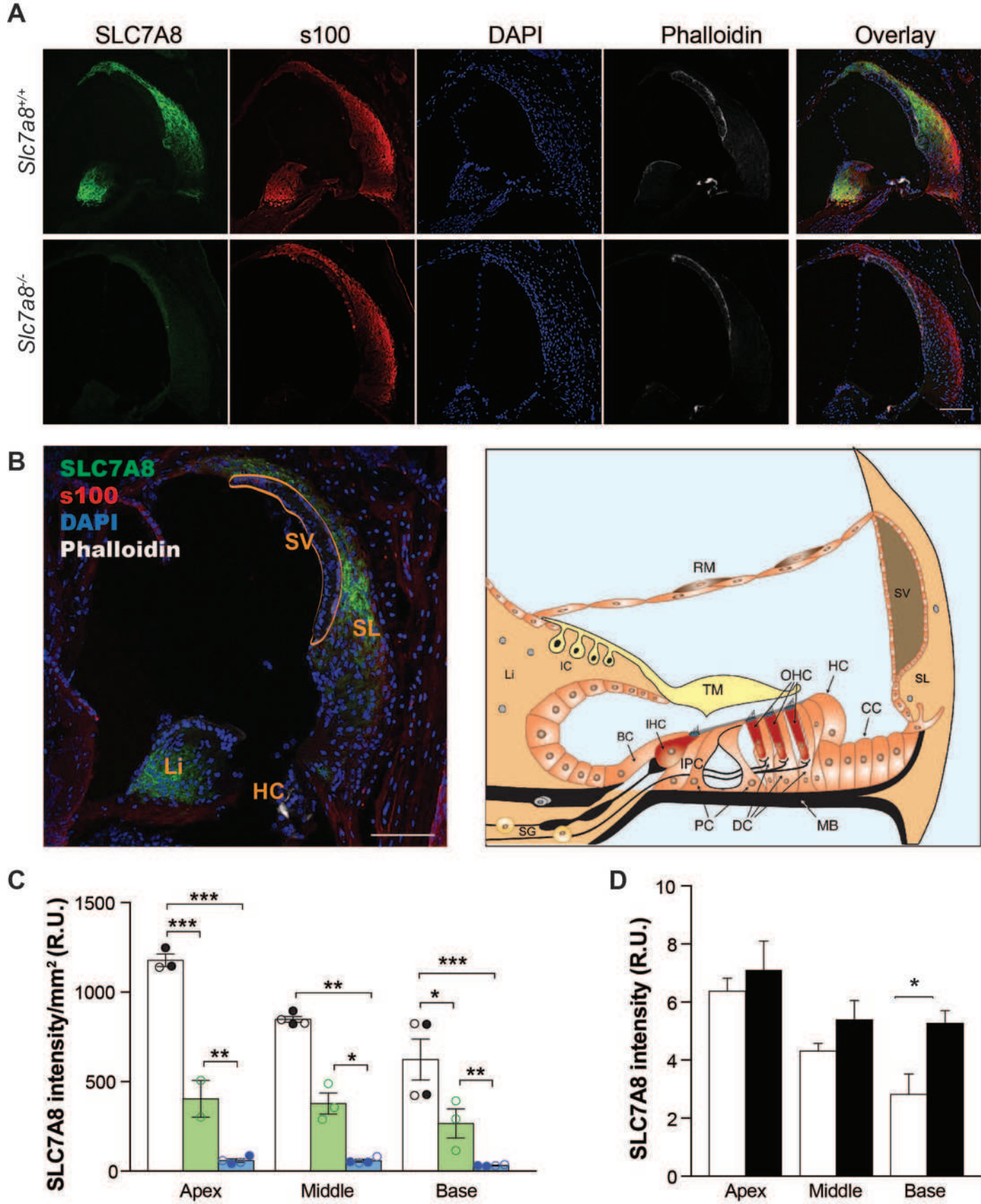
A
SLC7A8
s100
DAPI
Phalloidin
Overlay
Slc7a8+/+
Slc7a8-/-
B
SLC7A8
s100
DAPI
Phalloidin
SV
SL
Li
HC
RM
SV
Li
IC
TM
OHC
HC
SL
CC
IHC
BC
IPC
SG
PC
DC
MB
C
SLC7A8 intensity/mm² (R.U.)
1500
1000
500
0
***
***
**
**
*
***
*
**
Apex
Middle
Base
D
SLC7A8 intensity (R.U.)
10
8
6
4
2
0
*
Apex
Middle
Base

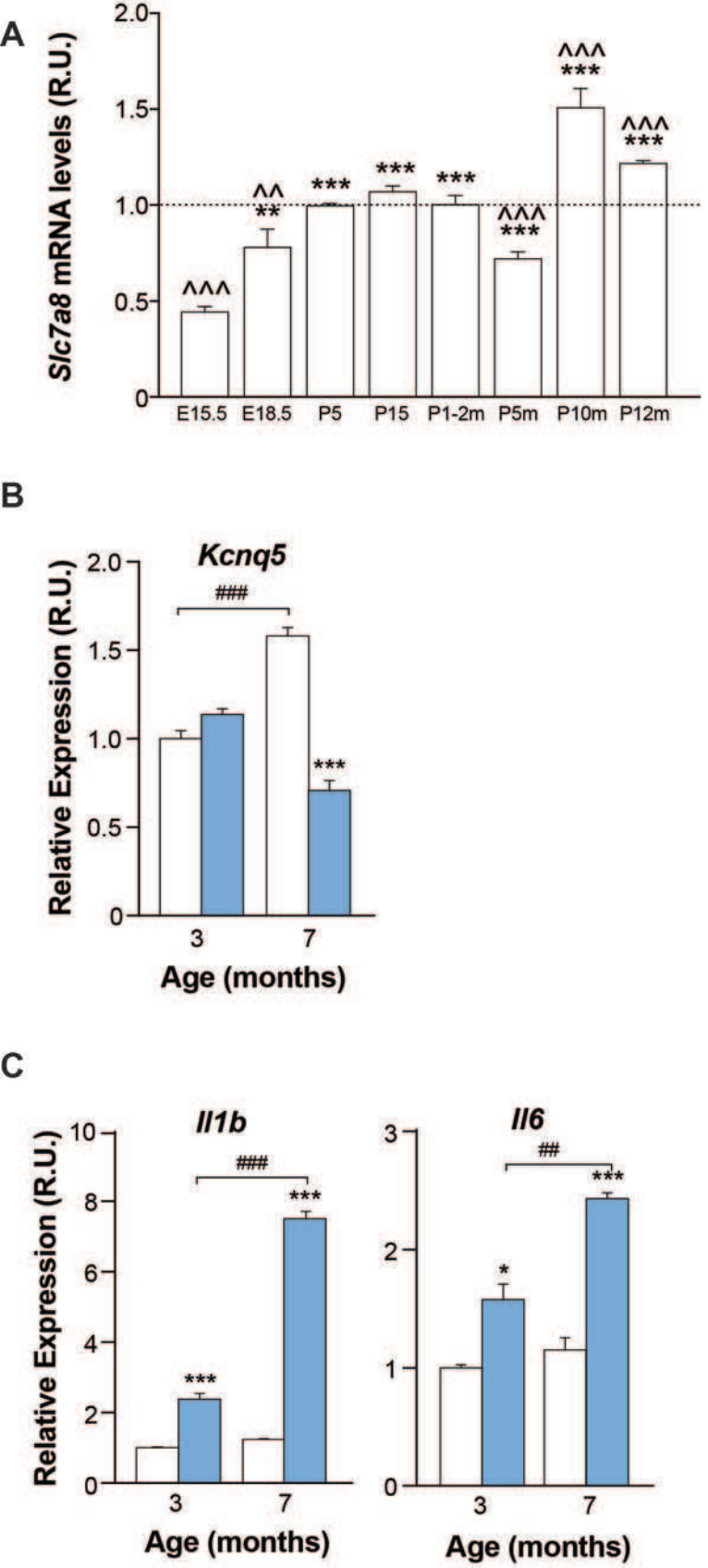
A
Slc7a8 mRNA levels (R.U.)
2.0
1.5
1.0
0.5
0
^^^
^^
**
***
***
***
^^^
***
^^^
***
^^^
***
E15.5
E18.5
P5
P15
P1-2m
P5m
P10m
P12m
B
Kcnq5
Relative Expression (R.U.)
2.0
1.5
1.0
0.5
0
###
***
3
7
Age (months)
C
Il1b
Relative Expression (R.U.)
10
8
6
4
2
0
###
***
***
3
7
Age (months)
Il6
3
2
1
0
##
***
*
3
7
Age (months)

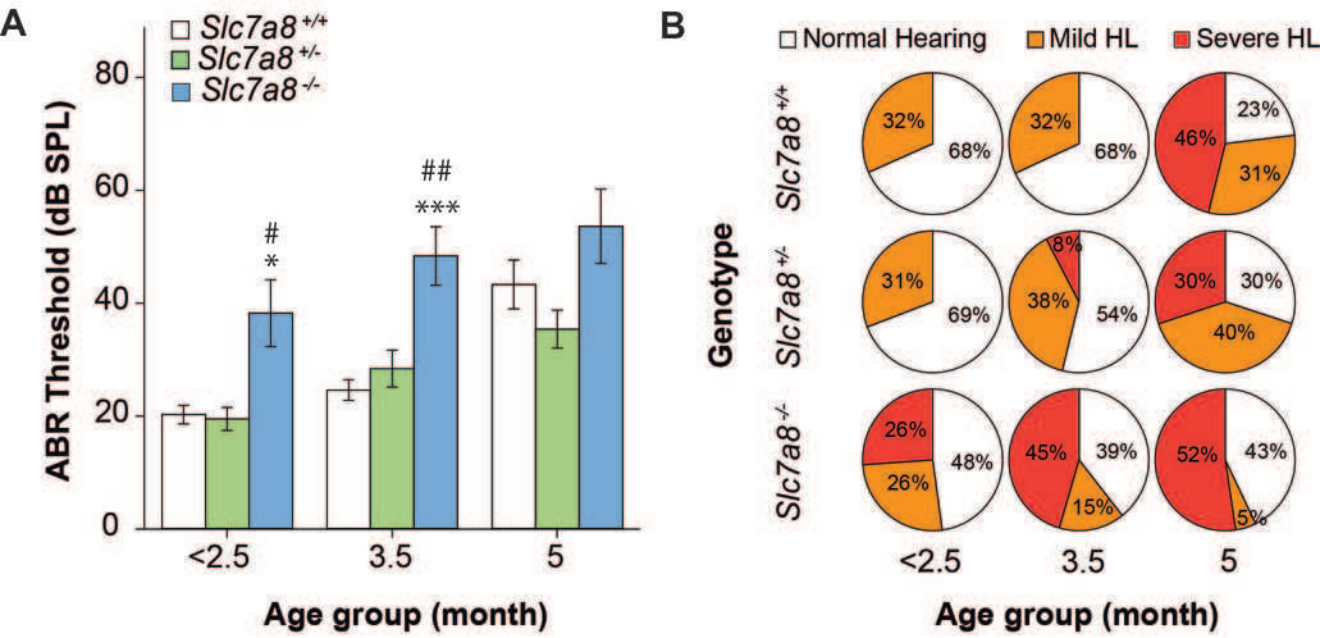
A
Slc7a8 +/+
Slc7a8 +/-
Slc7a8 -/-
ABR Threshold (dB SPL)
0
20
40
60
80
#
*
##
***
<2.5
3.5
5
Age group (month)
B
Normal Hearing
Mild HL
Severe HL
Genotype
Slc7a8 +/+
Slc7a8 +/-
Slc7a8 -/-
32%
68%
32%
68%
46%
23%
31%
31%
69%
8%
38%
54%
30%
30%
40%
26%
26%
48%
45%
39%
15%
52%
43%
5%
<2.5
3.5
5
Age group (month)

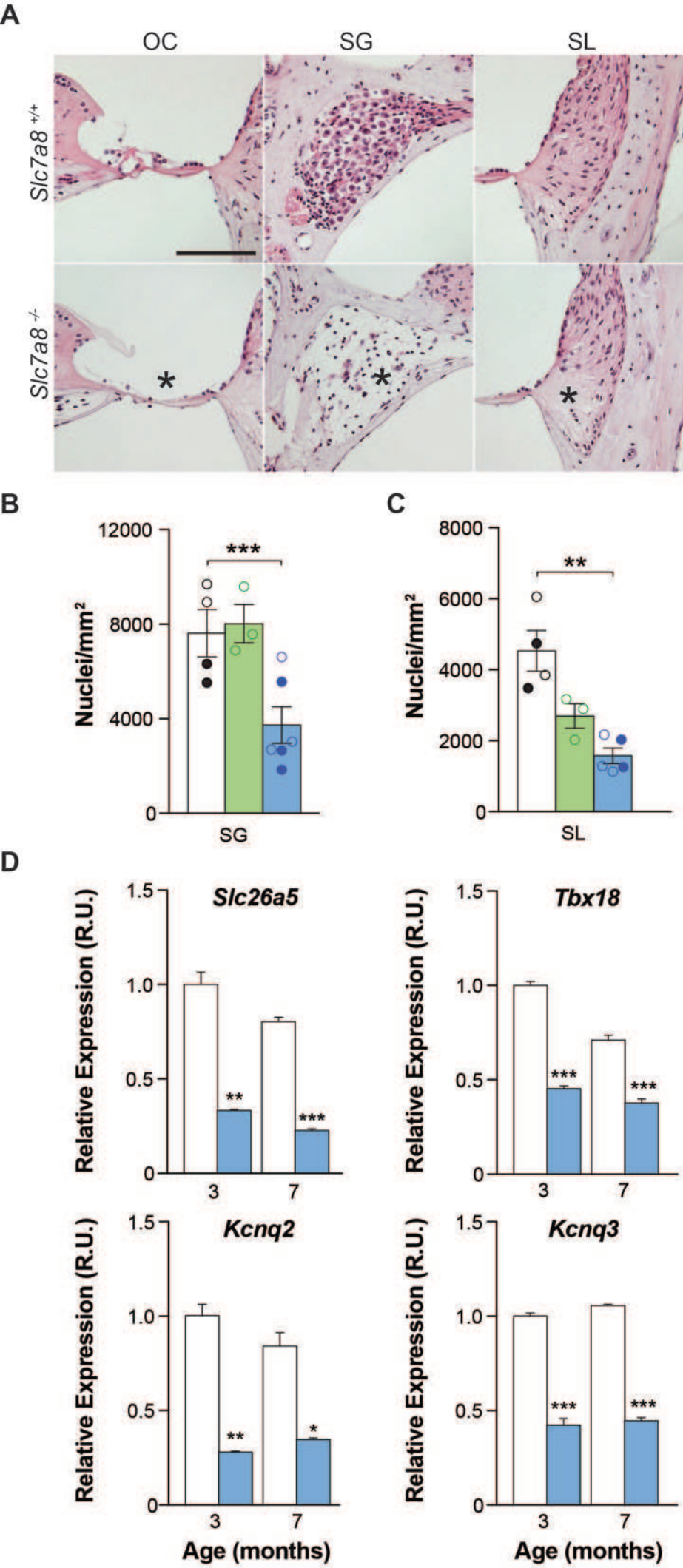
A
OC
SG
SL
Slc7a8 +/+
Slc7a8 -/-
*
*
*
B
12000
8000
4000
0
Nuclei/mm²
***
SG
C
8000
6000
4000
2000
0
Nuclei/mm²
**
SL
D
Slc26a5
Tbx18
Kcnq2
Kcnq3
Relative Expression (R.U.)
1.5
1.0
0.5
0
**
***
*
3
7
Age (months)

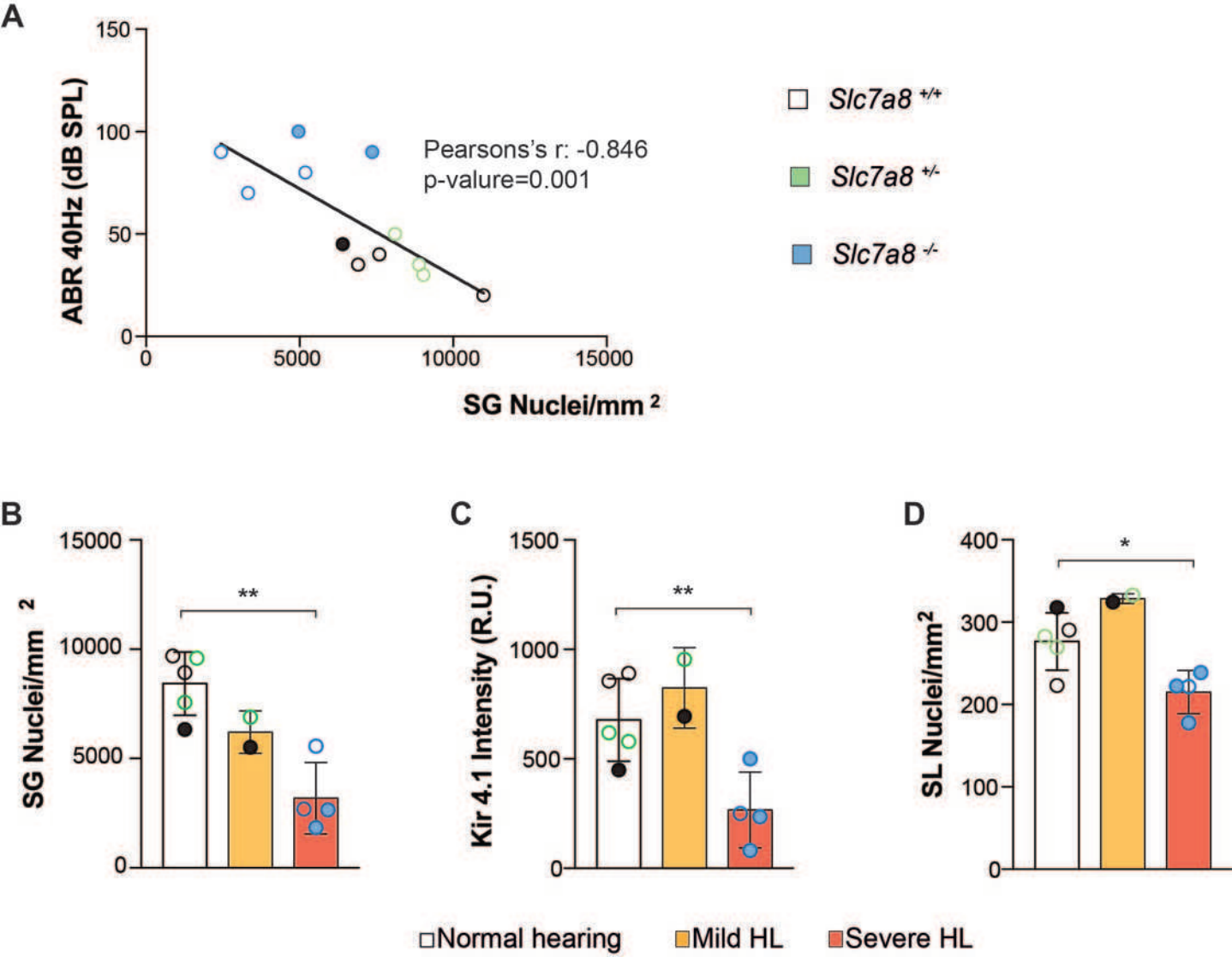
A
ABR 40Hz (dB SPL)
150
100
50
0
0
5000
10000
15000
SG Nuclei/mm 2
Pearsons's r: -0.846
p-value=0.001
Slc7a8 +/+
Slc7a8 +/-
Slc7a8 -/-
B
SG Nuclei/mm 2
15000
10000
5000
0
**
C
Kir 4.1 Intensity (R.U.)
1500
1000
500
0
**
D
SL Nuclei/mm2
400
300
200
100
0
*
Normal hearing
Mild HL
Severe HL

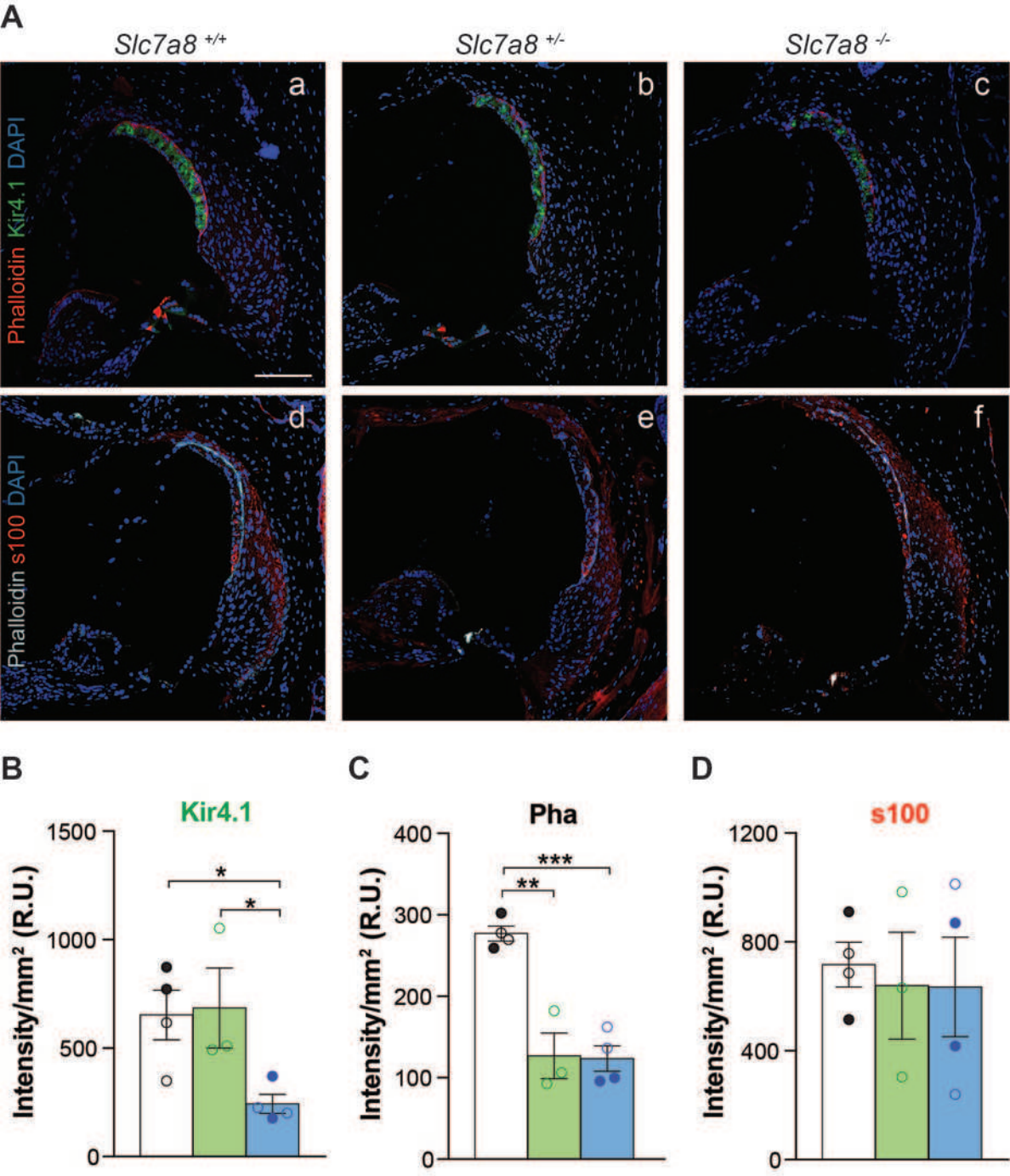
A
Slc7a8 +/+
Slc7a8 +/-
Slc7a8 -/-
a
b
c
d
e
f
Phalloidin Kir4.1 DAPI
Phalloidin s100 DAPI
B
Kir4.1
Intensity/mm² (R.U.)
1500
1000
500
0
*
*
C
Pha
Intensity/mm² (R.U.)
400
300
200
100
0
***
**
D
s100
Intensity/mm² (R.U.)
1200
800
400
0

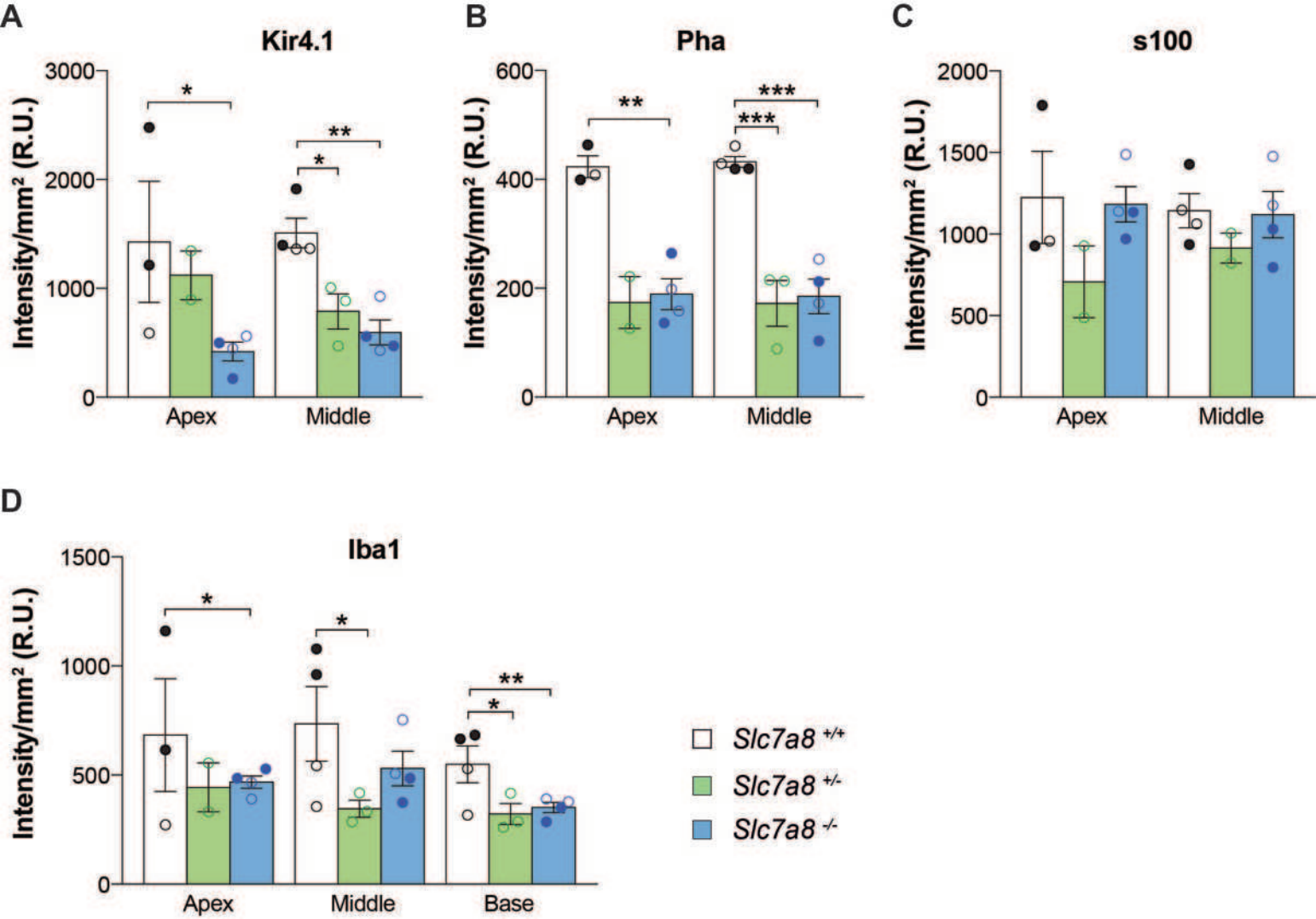
A
Kir4.1
Intensity/mm² (R.U.)
3000
2000
1000
0
*
**
*
Apex
Middle
B
Pha
Intensity/mm² (R.U.)
600
400
200
0
**
***
***
Apex
Middle
C
s100
Intensity/mm² (R.U.)
2000
1500
1000
500
0
Apex
Middle
D
Iba1
Intensity/mm² (R.U.)
1500
1000
500
0
*
*
**
*
Apex
Middle
Base
Slc7a8 +/+
Slc7a8 +/-
Slc7a8 -/-

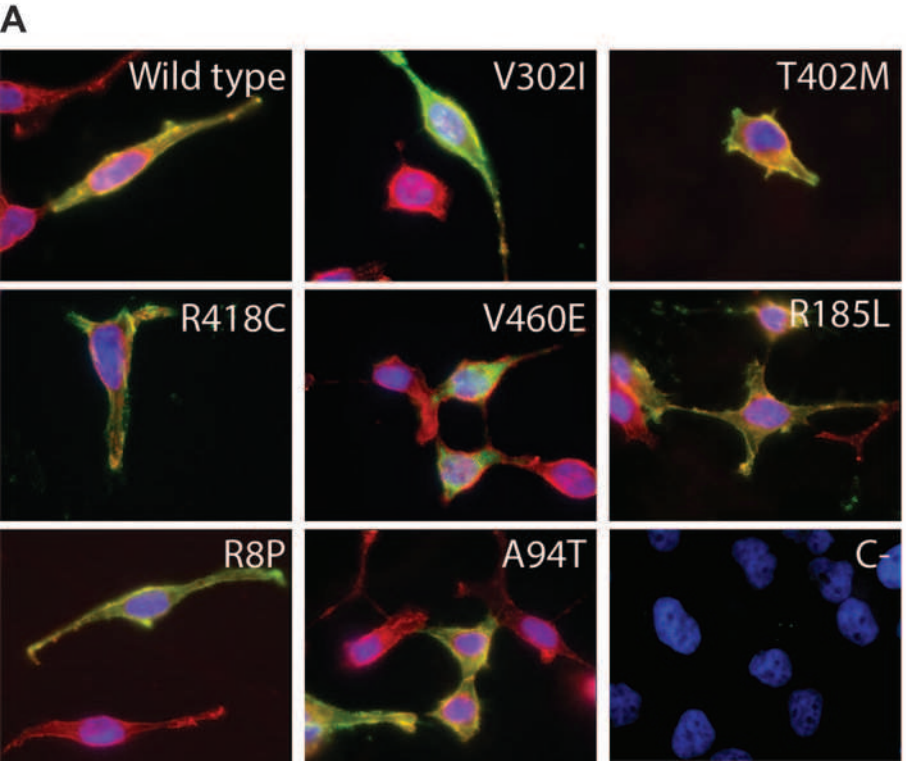
A
Wild type
V302I
T402M
R418C
V460E
R185L
R8P
A94T
C-

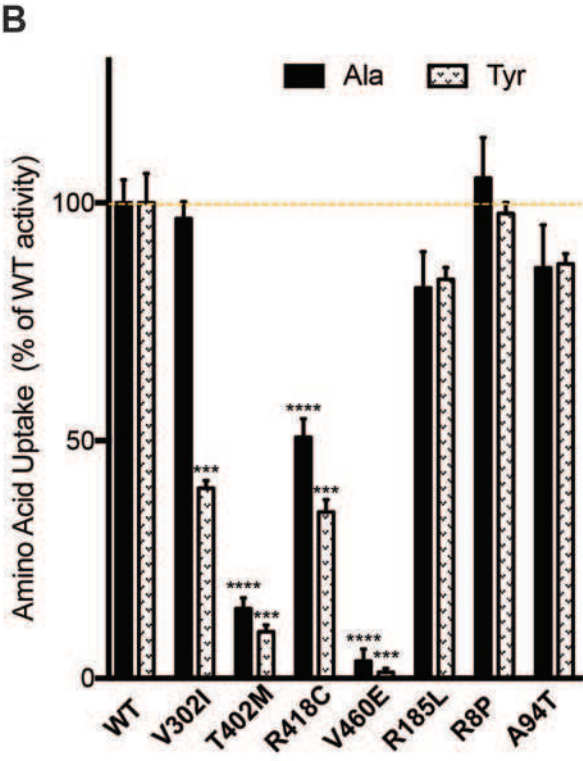
B
Ala
Tyr
Amino Acid Uptake (% of WT activity)
100
50
0
WT
V302I
T402M
R418C
V460E
R185L
R8P
A94T

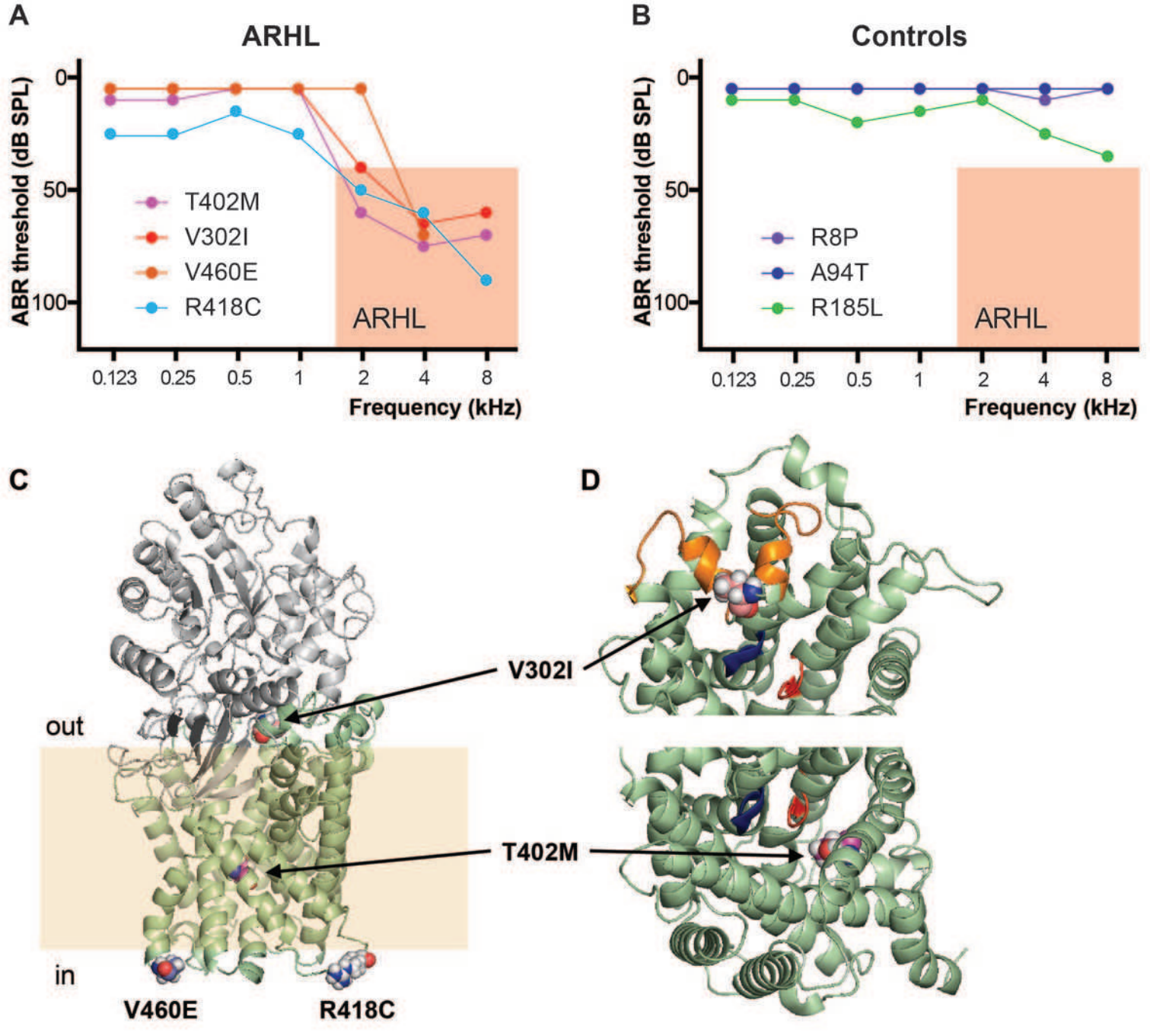
A
ARHL
ABR threshold (dB SPL)
0
50
100
T402M
V302I
V460E
R418C
ARHL
0.123
0.25
0.5
1
2
4
8
Frequency (kHz)
B
Controls
ABR threshold (dB SPL)
0
50
100
R8P
A94T
R185L
ARHL
0.123
0.25
0.5
1
2
4
8
Frequency (kHz)
C
out
in
V460E
R418C
V302I
T402M
D